HHS Public Access

Author manuscript

Nature. Author manuscript; available in PMC 2021 January 15.

Published in final edited form as:

Nature. 2020 September ; 585(7825): 397–403. doi:10.1038/s41586-020-2494-3.

Suppression of proteolipid protein rescues Pelizaeus-Merzbacher disease

Matthew S. Elitt[1], **Lilianne Barbar**[1], **H. Elizabeth Shick**[1], **Berit E. Powers**[2], **Yuka Maeno-Hikichi**[1], **Mayur Madhavan**[1], **Kevin C. Allan**[1], **Baraa S. Nawash**[1], **Artur S. Gevorgyan**[1], **Stevephen Hung**[1], **Zachary S. Nevin**[1], **Hannah E. Olsen**[1], **Midori Hitomi**[3], **Daniela M. Schlatzer**[4], **Hien T. Zhao**[2], **Adam Swayze**[2], **David F. LePage**[1], **Weihong Jiang**[1], **Ronald A. Conlon**[1], **Frank Rigo**[2], **Paul J. Tesar**[1,*]

[1]Department of Genetics and Genome Sciences, Case Western Reserve University School of Medicine, Cleveland, Ohio 44106, USA.

[2]Ionis Pharmaceuticals, Carlsbad, California 92008, USA.

[3]Lerner Research Institute, Cleveland Clinic, Cleveland, Ohio 44106, USA.

[4]Case Center for Proteomics and Bioinformatics, Department of Medicine, Case Western Reserve University School of Medicine, Cleveland, Ohio 44106, USA.

Abstract

Mutations in *proteolipid protein 1* (*PLP1*) result in failure of myelination and neurological dysfunction in the X-linked leukodystrophy Pelizaeus-Merzbacher disease (PMD)[1,2]. Most *PLP1* mutations, including point mutations and supernumerary copy variants, lead to severe and fatal disease. *PLP1*-null patients and mice, however, can display comparatively mild phenotypes, suggesting that *PLP1*-suppression might provide a general therapeutic strategy for PMD[1,3–5]. Here we show effective *in vivo Plp1*-suppression in the severe *jimpy* (*Plp1*^{jp}) point mutation mouse

* paul.tesar@case.edu.

Author contributions M.S.E. and P.J.T. conceived and managed the overall study. H.E.S and M.S.E. maintained the animal colonies and tracked survival. M.S.E. captured video recordings. L.B. and M.S.E. designed and tested sgRNAs. S.H. performed data analysis for CRISPR off-target assessments. D.F.L., R.A.C., and W.J. performed zygote electroporation and oviduct transfers. H.E.S., B.S.N., K.C.A., and L.B. performed western blot experiments and protein quantitation. D.M.S. and H.E.S. performed mass spectrometry sample preparation and analysis. B.E.P, L.B., B.S.N., and K.C.A. performed qRT-PCR. M.M., B.S.N, L.B., H.E.S., A.S.G, and M.S.E. generated and quantified the immunohistochemistry data. Y.M. performed optic nerve electrophysiology studies and analyzed the data. Y.M., M.H., M.S.E, and H.E.S. processed samples for electron microscopy. Y.M. analyzed and quantified electron microscopy images. M.S.E, K.C.A., B.S.N., and L.B. performed rotarod and open field experiments. M.S.E., B.S.N., K.C.A, and H.E.O. generated and characterized iPSCs and OPCs *in vitro*. H.T.Z. and A.S. generated *Hdac2*-targeting ASO data. B.E.P. and F.R. designed and characterized *Plp1*-targeting ASOs, tested tolerability in adult mice, recommended the use of ASOs, and contributed to the study design and interpretation of results in the ASO-treated disease model. M.S.E. performed ASO injections in *jimpy* mice. Y.M. and B.S.N. performed all respiratory evaluations and analyzed the data. Z.S.N. contributed key components to experimental design, data analysis, and manuscript composition. M.S.E. and L.B. performed statistical analyses. M.S.E., M.M., Y.M., L.B., and P.J.T. assembled figures. M.S.E. and P.J.T. wrote the manuscript with input from all authors.

Competing interests P.J.T. and M.S.E. are listed as inventors on pending patent claims (PCT/US2017/064870) filed by CWRU covering methods of PLP1 suppression. P.J.T. is a co-founder and consultant for Convelo Therapeutics, which has licensed patents unrelated to the current study from CWRU inventors (P.J.T., M.S.E., Z.S.N., and M.M.). P.J.T. and CWRU retain equity in Convelo Therapeutics. P.J.T. is a consultant and on the Scientific Advisory Board of Cell Line Genetics, which performed karyotyping in this study. P.J.T. is Chair of the Scientific Advisory Board (volunteer position) for the Pelizaeus-Merzbacher Disease Foundation. B.E.P., H.T.Z., A.S., and F.R. are employees of Ionis Pharmaceuticals. No other authors declare competing interests.

model of PMD. CRISPR-Cas9 mediated germline suppression of *Plp1* in *jimpy* mice increased myelination and restored nerve conduction velocity, motor function, and lifespan to wild-type levels, validating *PLP1*-suppression as a therapeutic approach. To evaluate the translational potential of this strategy we identified antisense oligonucleotides (ASOs) that stably decrease *Plp1* mRNA and protein throughout the neuraxis, *in vivo*. Administration of a single dose of *Plp1*-targeting ASOs to postnatal *jimpy* mice fully restored oligodendrocyte numbers, increased myelination, improved motor performance, normalized respiratory function, and extended lifespan through an 8-month endpoint. These results support the development of *PLP1*-suppression as a treatment for PMD. More broadly, we demonstrate that oligonucleotide therapeutics can be delivered to oligodendrocytes *in vivo* to modulate neurological function and lifespan, establishing a new pharmaceutical modality for myelin disorders.

Pelizaeus-Merzbacher disease (PMD; MIM 312080) is a fatal, X-linked leukodystrophy characterized by extensive loss of myelinating oligodendrocytes in the central nervous system (CNS). Mutations in the *proteolipid protein 1* (*PLP1*; MIM 300401) gene, which codes for the highly conserved tetraspan, oligodendrocyte protein PLP, cause PMD[1,2]. Symptoms typically present connatally or in childhood, and include a constellation of nystagmus, spasticity, hypotonia, and cognitive dysfunction, with mortality often prior to adulthood. Preclinical efforts to extend lifespan have demonstrated only limited success, and no therapy has shown efficacy in patients[6–13].

Most PMD patients harbor *PLP1* duplication mutations, causing overexpression of otherwise normal PLP protein[1,2]. However, hundreds of unique PMD-causative point mutations, which result in abnormal PLP protein, have also been identified. Notably, rare *PLP1*-null patients display symptoms that are delayed and milder compared to those with more severe duplications or point mutations[3–5]. Null patients can live for 40–60 years, do not develop spastic paraparesis until the 2nd-3rd decade of life, and maintain intact cognition until the 3rd-4th decade of life (Supplementary Table 1), possibly explained by a lack of cellular stress responses and oligodendrocyte death triggered by excess or abnormal PLP[1,2,12,14,15].

This clinical landscape suggests several opportunities for therapeutic development. Specifically, reducing *PLP1* expression to normal levels in patients with gene duplications would theoretically be curative. More broadly, the milder presentation of null patients implies a wide therapeutic window for titrating *PLP1* expression, which could be leveraged to restore functional oligodendrocytes in point mutation patients who generate abnormal PLP. Here, we demonstrate therapeutic *Plp1*-supression using germline- and postnatal-based approaches in PMD mice expressing abnormal PLP.

Germline suppression of *Plp1* in PMD mice

To test if *Plp1*-suppression provides a generalizable therapeutic approach for PMD we utilized the *jimpy* (*Plp1*^{jp}) mouse model of PMD that expresses abnormal PLP and recapitulates the cellular, molecular, and neurologic features seen in severe PMD. We targeted *Plp1* with CRISPR[16,17], using guide RNAs (sgRNAs) with high on-target, germline cutting efficiency (Supplementary Table 2), to generate a CRISPR-modified *jimpy* (CR-*impy*) founder with a complex deletion in *Plp1* (Fig. 1a and Extended Data Fig. 1a–c). Prior

to subsequent analyses, rare off-target mutations were eliminated by backcrossing (Extended Data Fig. 1b, d–e).

While *jimpy* mice showed severe tremor, ataxia, seizures (lasting >30 seconds), and death by the third postnatal week, CR-*impy* demonstrated a 21-fold increase in lifespan (mean survival = 489 and 23 days for CR-*impy*, and *jimpy*, respectively) with no evidence of tremor, ataxia, or seizures through the terminal endpoint of 18 months of age (Fig. 1b, Supplementary Data 1, Supplementary Video 1, and Supplementary Video 2). CR-*impy Plp1* transcript was reduced by 61–74% relative to wild-type in multiple CNS regions at 6 months of age (Extended Data Fig. 2a), with undetectable PLP protein (Supplementary Table 3).

To explore the effects of germline *Plp1*-suppression on cellular pathology, we assessed for markers of oligodendrocyte lineage and neuroinflammation. The mature myelin marker myelin basic protein (MBP) was grossly and stably restored to near wild-type levels throughout the neuraxis in CR-*impy* (Fig. 1c). In contrast to nearly nonexistent *Mbp* expression in *jimpy*, CR-*impy* demonstrated substantially increased transcript (83–91% of wild-type at 6 months of age) and protein (40–95% and 114–130% of wild-type at 3 weeks and 6 months of age, respectively) in multiple CNS regions (Extended Data Fig. 2b–d, Supplementary Data 2a–b, and Supplementary Data 3–5). Quantification of myelin regulatory factor (MyRF) positive oligodendrocytes showed their complete restoration throughout multiple CNS regions in CR-*impy* (94–117% and 89–126% of wild-type at 3 weeks and 6 months of age, respectively), contrasted by their depletion in *jimpy* (36–59% of wild-type at 3 weeks of age) (Fig. 1d–e and Supplementary Data 3–5). The glial lineage marker SOX10, which is expressed by oligodendrocytes and oligodendrocyte progenitor cells (OPCs), showed no differences across genotypes (Fig. 1d–e and Supplementary Data 3–5). CR-*impy* showed minimal evidence of astrogliosis or microglial activation through 6 months of age, in contrast to elevated neuroinflammatory markers in *jimpy*[18] (Extended Data Fig. 3a–d and Supplementary Data 3–5).

To investigate *Plp1*-suppression in oligodendrocytes isolated from cell-extrinsic developmental or inflammatory cues, we generated and characterized induced pluripotent stem cell (iPSC) lines (Extended Data Fig. 4a–b), which were differentiated to oligodendrocytes *in vitro*. Notably, CR-*impy* lines showed cell type-specific rescue in oligodendrocyte number and arborized morphology relative to *jimpy* (Extended Data Fig. 4c–g). Collectively, these data confirm that *Plp1*-suppression has a cell-intrinsic effect on oligodendrocytes that is sufficient to rescue *jimpy* cellular phenotypes.

To assess the effect of germline *Plp1*-suppression on myelination we quantified electron micrograph data. In contrast to nearly absent myelination in *jimpy*, CR-*impy* demonstrated a profound increase in myelinated axons throughout the neuraxis, reaching nearly 50% of wild-type at 3 weeks of age, with stability through 18-months (Fig. 1f–h). CR-*impy* myelin sheaths showed incomplete compaction compared to wild-type, consistent with PLP's role in myelin ultrastructure (Fig. 1f–g)[5,19]. To determine if CR-*impy* myelin was functional, we measured compound action potential speed in the optic nerve. At 3 weeks of age, we found a significant increase in conduction velocity in CR-*impy* relative to *jimpy* (Fig. 1i) (reaching ~55% of wild-type), which was well-correlated with the level of myelination in CR-*impy*

(~35% of wild-type) (Fig. 1j). Notably, CR-*impy* and wild-type showed comparable conduction velocities at 6 months of age (Fig. 1i).

To determine whether restored myelin altered complex motor function, we used longitudinal open-field and rotarod testing. Overall locomotion was decreased in *jimpy* mice, but similar between CR-*impy* and wild-type mice across all time points (Fig. 1k). Rotarod testing revealed that CR-*impy* mice showed similar performance to wild-type mice up to 6 months of age, whereas *jimpy* mice exhibited significant impairment. At 18 months of age, the CR-*impy* mice displayed slightly reduced performance (Fig. 1l), potentially reflecting late-onset neuronal phenotypes [REFERENCE 4]. Together, these results establish that germline suppression of *Plp1* restores oligodendrocytes, functional myelin and lifespan in *jimpy* mice.

In vivo suppression of oligodendrocyte transcripts

After validating *Plp1* as a therapeutic target for PMD using germline suppression, we pursued a clinically translatable strategy for *in vivo*, postnatal *Plp1*-suppression using newer generation antisense oligonucleotides (ASOs). These ASOs, characterized by highly-efficient modulation of CNS target transcripts with multi-month *in vivo* half-lives, underlie several therapies for fatal neuronal-based disorders[20–22], however their ability to target the oligodendrocyte lineage *in vivo* was unknown. To establish their therapeutic potential for this lineage, we administered well-characterized ASOs targeting *Hdac2*, whose nuclear localized protein product enables clear visualization of target suppression, to adult wild-type mice by intracerebroventricular (ICV) injection, demonstrating a substantial reduction of HDAC2 in oligodendrocytes and OPCs (Fig. 2a–b). Next we identified two independent ASOs targeting the 5th intron (ASO*Plp1*.a) and 3'UTR (ASO*Plp1*.b) of *Plp1* (Fig. 2c), along with a non-targeting ASO control (ASOctr), which we administered to wild-type mice (wtASO*Plp1.a* and wtASO*Plp1.b*, and wtASOctr, respectively). ASOs exhibited dose-dependent suppression of *Plp1* transcript (up to 90% and 98% in neonatal and adult wild-type mice, respectively) and PLP protein (up to 63% in neonatal wild-type mice) in multiple CNS regions (Fig. 2d–g, Extended Data Fig. 5a). ASOs distributed widely across the neuroaxis, lacked significant off-targeting, and did not affect wild-type MBP protein levels (Extended Data Fig. 5b–h, 6a–b, 7a, and Supplementary Data 7a).

Postnatal *Plp1*-suppression in PMD mice

We evaluated the therapeutic effect of *Plp1*-targeting ASOs on the severe *jimpy* phenotype using a single ICV injection at birth (Fig. 3a). Remarkably, *jimpy* mice injected with ASO *Plp1*.a (jpASO*Plp1*.a) or ASO *Plp1*.b (jpASO*Plp1*.b) demonstrated a ~12-fold (jpASO*Plp1*.a) and ~11-fold (jpASO*Plp1*.b) increase in lifespan compared to ASO control-injected *jimpy* (jpASOctr) (mean survival = 20, 239, and 217 days for jpASOctr, jpASO*Plp1*.a, and jpASO*Plp1*.b, respectively) through a predetermined terminal endpoint of 8 months of age (Fig. 3b, Supplementary Data 6, Supplementary Video 3, and Supplementary Video 4).

MBP expression was grossly increased in jpASO*Plp1*.a and jpASO*Plp1*.b relative to jpASOctr, through 8-months, without additional ASO dosing (Fig 3c–d). *Mbp* transcript and

MBP protein were significantly increased across the neuraxis in jpASO*Plp1*.a and jpASO*Plp1*.b relative to jpASOctr (up to a 39-fold increase in MBP protein), along with a concomitant reduction of apoptotic cells (Fig. 3c–d, Extended Data Fig. 7b–e, Supplementary Data 7b, and Supplementary Data 8–10). MyRF positive oligodendrocytes were restored throughout the neuraxis at 3 weeks of age in jpASO*Plp1*.a and jpASO*Plp1*.b (81–101% of wtASOctr), contrasted by their substantial depletion in jpASOctr (Fig. 3e and Supplementary Data 8–10). These trends were further validated using the orthogonal, oligodendrocyte marker set, CC1/OLIG2 (Extended Data Fig. 7f and Supplementary Data 11–13). SOX10 and OLIG2 positive oligodendrocyte lineage cells showed similar levels across groups (Fig. 3f, Extended Data Fig. 7g, and Supplementary Data 8–13). PDGFRα/OLIG2 double-positive OPCs, while comparable in wtASOctr, jpASO*Plp1*.a and jpASO*Plp1*.b, were elevated in jpASOctr (Extended Data Fig. 7h and Supplementary Data 11–13), suggesting a *jimpy*-specific compensatory increase in progenitors[23]. Myelinated axons were significantly increased throughout the neuraxis in jpASO*Plp1*.a and jpASO*Plp1*.b relative to jpASOctr at 3 weeks of age (~5 to 6-fold and 12 to 15-fold higher in the corpus callosum and brainstem, respectively) (Fig. 3g–h). While oligodendrocyte numbers were fully restored, this increased myelination reached ~10% of wtASOctr at 3 weeks of age and persisted through our terminal 8-month endpoint, albeit with less compaction (Fig. 3g–h and Extended Data 8a–b).

Strikingly, jpASO*Plp1*.a and jpASO*Plp1*.b showed only minor *jimpy* phenotypes, including markedly reduced tremor and occasional short duration seizures (<15 seconds), but otherwise appeared overtly normal in daily activities, including the ability to breed (Supplementary Data 6). While rotarod performance was only variably and partial improved in jpASO*Plp1*.a and jpASO*Plp1*.b (to a maximum of 36% of wild-type), overall locomotion was restored to wild-type levels across multiple time points (Fig. 4a–b). To assess whether myelin could be contributing to these functional improvements we measured compound action potential speed in the optic nerve. At 3 weeks of age we found a modest but significant increase in conduction velocity in jpASO*Plp1*.b versus jpASOctr (Fig. 4c), representing ~17% of wtASOctr levels, which directly correlated with the level of myelination relative to wtASOctr (~10%) (Fig. 4d). Together these data demonstrate that a single postnatal administration of *Plp1*-targeting ASOs elicits a sustained reduction in *Plp1* expression that restores oligodendrocytes and increases functional myelin, with improvements in motor performance and lifespan in *jimpy*.

Respiratory distress and dysfunction has been associated with premature death in PMD models and patients[24–27], which is notable given the profound increase in survival of jpASO*Plp1*.a and jpASO*Plp1*.b in light of the relatively modest increases in myelin globally, with the highest levels consistently observed in the brainstem (Fig. 3g–h and Extended Data 7b–c). Interestingly, brainstem respiratory control centers alter breathing patterns in response to physiologic derangements seen during hypoxia or hypercapnia. Seizures, as observed in *jimpy* mice beginning around the third postnatal week, can trigger such derangements (Fig. 4e) and, when coupled with a reduced capacity to achieve homeostasis, could be lethal.

To explore whether respiratory function is a therapeutic component of *Plp1*-targeting ASOs, we used plethysmography to measure minute ventilation in normal air, hypercapnic (5% CO_2), and hypoxic (10.5% O_2) conditions (Supplementary Data 14). When transitioned from normal air to either hypercapnic or hypoxic environments, jpASOctr exhibited high variability in minute ventilation, indicative of dysfunctional respiratory control (Fig. 4f) while jpASO*Plp1*.b showed less variability, and magnitudes of response more similar to wtASOctr (Fig. 4f–j). Specifically, jpASOctr showed weak compensatory decrease in minute ventilation when exposed to hypercapnic conditions relative to wtASOctr, which was restored in jpASO*Plp1*.b (Fig. 4g–h). During early transition to hypoxia, wtASOctr and jpASO*Plp1*.b demonstrated similar compensatory increases in minute ventilation while jpASOctr showed a blunted response (Fig. 4g, i). In extended hypoxia, jpASOctr showed an exaggerated decrease in minute ventilation relative to wtASOctr, which was restored in jpASO*Plp1*.b (Fig. 4j). Strikingly, during this hypoxic challenge, 38% of jpASOctr died spontaneously while 100% of jpASO*Plp1*.b and wtASOctr survived (Fig. 4k). Together, these results suggest that dysregulated control of respiration is a component of the *jimpy* phenotype and potentially underlies the premature mortality that occurs coincident with the onset of seizures, which can be partially rescued by suppression of *Plp1*.

Discussion

In summary, we have validated a clinically feasible therapeutic strategy for PMD based on a mutation-agnostic, *PLP1*-suppression approach. We demonstrate both CRISPR-Cas9 germline-based and postnatal ASO-mediated suppression of *Plp1* expression that each result in rescue of major PMD phenotypes in a severe PMD mouse model. Furthermore, we establish oligonucleotide-based drugs, delivered postnatally, to modulate a disease target in oligodendrocytes and restore both functional myelin and lifespan in a fatal genetic disorder.

This study provides the foundational data for the development of clinically relevant ASO technology to achieve postnatal reduction of *Plp1*. While additional preclinical development is needed to optimize dosage and timing, including treating later in disease, our results highlight that even a single ASO injection can elicit a sustained phenotypic improvement relative to the natural history of the disease, even with only ~10% of myelin restored relative to wild-type. These data could reflect a previously unappreciated functional tolerance to incomplete myelination or may be indicative of a neuronal supportive function of the oligodendrocytes[28–30], whose levels were completely restored in *jimpy* injected with *Plp1*-targeting ASOs.

Complete elimination of mutant PLP could convert severe PMD patients to a *PLP1*-null phenotype, characterized by milder disease that presents later, progresses slower, and shows improved clinical outcomes[1,3–5]. Importantly, titration of abnormal or excessive PLP to a level that relieves cellular stress-mediated oligodendrocyte death but maintains PLP's neuronal supportive function[3–5,19] could potentially supersede this benefit. This strategy would be especially amendable to the 70% of PMD patients who harbor gene duplications leading to excess, but otherwise normal, PLP protein[1], as a reduction to wild-type levels of *PLP1* expression may be curative.

Collectively our studies, combined with the feasibility of ASO delivery to the human CNS and current safety data in other CNS indications, support advancement of *PLP1*-suppression into the clinic as a therapeutic with potential applicability across the spectrum of PMD patients. More broadly, our data provide a framework for transcript modulation in oligodendrocytes to restore myelination in genetic and sporadic disorders of myelin.

Methods

All data was reproduced with biological replicates as indicated. Blinding was employed, as indicated. No statistical methods were used to predetermine sample size and the experiments were not randomized. p-values stated for $p<0.1$, otherwise not significant (n.s).

Mice

All procedures were in accordance with the National Institutes of Health Guidelines for the Care and Use of Laboratory Animals and were approved by the Case Western Reserve University Institutional Animal Care and Use Committee (IACUC).

Wild-type (B6CBACa-Aw-J/A) and *jimpy* (B6CBACa-Aw-J/A-Plp1jp EdaTa/J; RRID:IMSR_JAX:000287) mice used in this study were purchased from Jackson Laboratory (Bar Harbor, ME). *Jimpy* males possess a point mutation in the splice acceptor site of *Plp1* intron 4 (c.623–2A>G), which results in exclusion of exon 5 and a frameshift of the final 70 amino acids of PLP[31]. The colony was maintained by breeding heterozygous females, which lack a phenotype, to wild-type males to generate affected *jimpy* males. Mice were housed under a temperature-controlled environment, 12-h light-dark cycle with ad libitum access to water and rodent chow. All mice were genotyped approximately a week after birth using genomic DNA isolated from tail tips or toes at two loci: 1) the *jimpy* mutation (NM_011123.4:c.623–2A>G) in *Plp1* intron 4, which causes skipping of exon 5 and a truncated PLP protein and 2) the complex indel in *Plp1* exon 3 from dual cutting of CRISPR/Cas9 sgRNAs in CR-*impy* mice (c.[242_318del; 328_330del]). This causes a frameshift in *Plp1*, a premature stop codon in exon 4, and is predicted to cause nonsense mediated decay of the transcript and loss of protein. Genotyping was performed by standard Sanger sequencing or a custom real time PCR assays (Probe identifiers: Plp1–2 Mut [for *jimpy* mutation in intron 4] and Plp1–5 WT [for CR-*impy* complex deletion in exon 3], Transnetyx, Cordova, TN).

Primers for Sanger sequencing provided in Supplementary Table 4.

Plp1-targeting sgRNA design

Mouse *Plp1* sequence was entered into the *Streptococcus pyogenes* clustered regularly interspaced short palindromic repeat-associated 9 (CRISPR-spCas9) sgRNA design tool at crispr.mit.edu[32] and analyzed against the mm10 target genome. *Plp1*-targeting sgRNAs were sorted based on their on-target efficiency while minimizing off-target mutations. On-target nuclease activity was confirmed for each sgRNA using the Guide-it sgRNA Screening Kit (631440, Clontech) according to the manufacturer's instructions. The following sgRNAs were tested:

sgRNA1: CCCCTGTTACCGTTGCGCTC

sgRNA2: TGGCCACCAGGGAAGCAAAG

sgRNA3: AAGACCACCATCTGCGGCAA

sgRNA4: GGCCTGAGCGCAACGGTAAC

sgRNA5: GCCTGAGCGCAACGGTAACA

sgRNA6: TCTACACCACCGGCGCAGTC

sgRNA7: CCAGCAGGAGGGCCCCATAA

sgRNA8: GAAGGCAATAGACTGACAGG

This list was further filtered based on the ability of each sgRNA to target *Plp1*'s splice isoform *Dm20*, in addition to *Plp1*. We selected two sgRNAs (3 and 7) that targeted exon 3 of *Plp1* for combined use in zygote studies, which enabled the rapid detection of large deletion events by PCR and provided redundancy for on-target cutting.

Suppression of *Plp1* in *jimpy* zygotes using CRISPR-Cas9

Carrier female oocyte donors were administered 5 IU pregnant mare's serum gonadotropin by intraperitoneal injection (G4877, Sigma-Aldrich), followed by 2.5 IU human chorionic gonadotropin (GC10, Sigma-Aldrich) 48 hours later. These superovulated females were mated to wild-type males. Zygotes were harvested in FHM medium (MR-025 Sigma-Aldrich) with 0.1% hyaluronidase (H3501, Sigma-Aldrich) and the surrounding cumulus cells were separated. The zona pellucida of each zygote was partially dissected using 0.3M sucrose (S7903, Sigma-Aldrich) in FHM as previously described[33].

Zygotes were placed in 2x KSOM medium (MR-106, Sigma-Aldrich) with an equal volume of solution containing 100ng/μL sgRNA3, 100ng/μL sgRNA7 (AR01, PNAbio), and 200ng/μL spCas9 mRNA (CR01, PNAbio). Given the low frequency of *jimpy* zygotes and unknown *in vivo* targeting of the sgRNAs, both sgRNAs were used simultaneously to maximize the chance of *Plp1* frameshift. Electroporation was performed in a chamber with a 1mm gap between two electrodes using an ECM 830 Square Wave Electroporation System (BTX). Electroporation parameters were set as follows: 32V, 3ms pulse duration, 5 repeats, and 100ms inter-pulse interval. Electroporated zygotes were moved to KSOM medium and then transferred into the oviducts of pseudopregnant females (CD1). Electroporation settings were optimized to achieve maximal cutting efficiency in a separate strain but resulted in a higher rate of embryo loss in our B6CBACa/J strain. Zygotes were electroporated in batches of 54, 56, and 61, which resulted in 4, 3, and 0 pups born. The 7 surviving mice were genotyped after birth and monitored daily for onset of typical *jimpy* phenotypes including tremors, seizures, and early death by postnatal day 21. A founder *jimpy* male with complex deletion containing 80-bp of total deleted sequence in exon 3 of *Plp1*, denoted CR-*impy*, showed no overt phenotype and was backcrossed for two generations to the wild-type parental strain to reduce potential off-target Cas9 cutting effects (Extended Data Fig. 1b–e). A colony of mice was bred to evaluate cellular, molecular, and functional phenotypes of contemporaneous isogenic wild-type, *jimpy*, and CR-*impy* male mice. Mice were monitored daily to determine lifespan with statistical significance among groups determined using the

log-rank test. Additionally, animals surviving beyond 3 weeks were analyzed using behavioral (rotarod and open field testing for motor performance), histology (immunostaining of the CNS for myelin proteins and electron microscopy for myelin ultrastructure), and electrophysiology (conduction velocity of the optic nerve). Details and metadata for all mice in this study including censoring of animals in the survival analysis are found in Supplementary Data 1.

CRISPR on- and off-target assessment

CRISPR on-target cutting efficiencies were assessed by high throughput sequencing. PCR primers were designed to encompass each guide on-target site. Primer sequences were generated using NCBI Primer-BLAST and are provided in Supplementary Table 4. The following tails were added to the primer sequences:

Forward: TCCCTACACGACGCTCTTCCGATCT

Reverse: AGTTCAGACGTGTGCTCTTCCGATCT

PCR amplification on tail-tip genomic DNA was performed using the KAPA HiFi HotStart ReadyMix (07958935001, Roche) to minimize PCR-based error. Libraries were prepared by adding unique indices by PCR using KAPA HiFi HotStart ReadyMix. All libraries were pooled evenly and quantified using NEBNext® Library Quant Kit for Illumina® (E7630, New England Biolabs) then denatured and diluted per Illumina's MiSeq instructions. 250bp paired-end sequencing was performed using an Illumina MiSeq at the Case Western Reserve University School of Medicine Genomics Core Facility. Reads were compared against the consensus sequence and CRISPR-induced indel percentages were determined using the OutKnocker tool at outknocker.org[34].

Genomic DNA was isolated from brain tissue from the CR-*impy* founder male, three F2 generation CR-*impy* male mice (each from a unique breeding pair using independent F1 generation carrier females), and a *jimpy* male from a contemporaneous but independent cohort in our colony. Libraries were prepared for whole genome sequencing using Nextera DNA Flex Library prep (20018705, Illumina) and 150bp paired-end sequencing was performed using an Illumina NovaSeq. Reads were aligned to the mouse genome (mm10) using BWA[35] (version 0.7.17-r1188) with default parameters for paired reads. Local indel realignment was performed using GATK RealignerTargetCreator and IndelRealigner (version 3.3–2-gec30cee) at the on-target and off-target sites. Reads aligned to the window chrX:136831817–136832360 at the *Plp1* locus were re-aligned using Blat (v. 36×2) to fully capture the CR-*impy* complex deletion.

The top 50 potential off-target sites for each sgRNA were identified using the CCTop - CRISPR/Cas9 target online predictor tool[36], with a maximum total mismatch number of 4. Additionally, each site was identified using the RGEN Cas-OFFinder[37] and CRISPOR[38] off-target prediction algorithms, providing two independent validations of this off-target location list. The indel-realigned reads were visually inspected in Integrative Genomics Viewer (IGV)[39], and indels occurring at a frequency of at least 5% after filtering known polymorphisms from dbSNP (build 142) at these 50 potential off-target sites were considered CRISPR-induced mutations.

Video recording of mouse phenotypes

All recording was performed using video recording function on an Apple iPhone. Videos were color corrected, stabilized, and trimmed to a discrete range using Apple iMovie. Videos were collated and converted to MP4 format using Adobe After Effects.

Immunohistochemistry

Mice were anesthetized with isoflurane and sacrificed by transcardial perfusion with PBS followed by 4% PFA. Tissue was harvested and placed in 4% PFA overnight at 4°C. Samples were rinsed with PBS, equilibrated in 30% sucrose, and frozen in Tissue-Tek® Optimum Cutting Temperature compound (O.C.T.; 25608–930, VWR). Samples were cryosectioned at a 20μm thickness. Sections were washed in phosphate-buffered saline (PBS) and incubated overnight in antibody solution containing 2.5% normal donkey serum (NDS; 017-000-121, Jackson Labs) and 0.25% Triton X-100 (T8787, Sigma).

Alternatively, as noted elsewhere in the methods, mice were sacrificed by CO_2 asphyxiation, followed by tissue harvesting, emersion fixation overnight in 10% neutral buffered formalin, and paraffin embedding. Sections 5 μm thick were cut onto charged glass slides and dried overnight at 60°C. Sections were deparaffinized and hydrated using graded concentrations of ethanol to deionized water. Sections were subjected to antigen retrieval by sodium citrate buffer at pH 6 (H-3300; Vector Laboratories) at 100˚C for 45 min, gently washed in deionized water, and then transferred into 0.05 M Tris-based solution in 0.15 M NaCl with 0.1% (v/v) Triton X-100, pH 7.6 (TBST). For chromagen staining, endogenous peroxidase was blocked with 3% hydrogen peroxide for 20 min. Nonspecific background staining was blocked in 3% normal goat serum for 30 min (Sigma) at room temperature. For mouse antibodies, sections were incubated for 30 min in Mouse Blocking Reagent (Vector Laboratories). All slides were then incubated at 4°C overnight with cocktails of primary antibodies in TBST. For DAB reactions, after washing with TBST, sections were then incubated with the species-appropriate immunoglobulin G (IgG)-horseradish peroxidase (HRP) (1:300, SC2004; Santa Cruz), then reacted with diaminobenzidine (DAB; ScyTek Laboratories, Logan, UT) and counterstained with hematoxylin (no. 7211; Richard-Allen Scientific).

Sections were stained using the following antibodies at the indicated concentrations or dilutions: mouse anti-MBP (2μg/mL; 808401, Biolegend; RRID:AB_2564741), rabbit anti-MBP (1:1000; Abcam, ab40390; RRID:AB_1141521), rabbit anti-MyRF polyclonal antibody (1:500; kindly provided by Dr. Michael Wegner), goat anti-SOX10 (0.4μg/mL; AF2864, R&D Systems; RRID:AB_442208), rabbit anti-GFAP (1:1000; Z0334, Dako; RRID:AB_10013382), goat anti-IBA1 (0.1mg/mL; ab5076, Abcam), rabbit anti-IBA1 (1:2000; 019–19741, WAKO; RRID:AB_839504), rabbit anti-ASO (1:2500; Ionis Pharmaceuticals, Carlsbad, CA), rabbit anti-HDAC2 (1:250; Abcam, ab16032; RRID:AB_2118543), mouse anti-APC/CC1 (2.5 μg/ml; ab16794, Abcam; RRID:AB_443473), mouse anti-APC/CC1 (1:250; MABC200, Millipore; RRID:AB_11203645), rat anti-NG2 (25 μg/mL; MAB6689, R&D Systems; RRID:AB_10890940), goat anti-PDGFRα (1:500; AF1062, R&D systems; RRID:AB_2236897), and rabbit anti-OLIG2 (1:250; 13999–1-AP, ProteinTech;

RRID:AB_2157541). For MBP immunohistochemistry, sections were post fixed in methanol at −20°C for 20 minutes followed by overnight incubation in a PBS based primary antibody solution containing 0.1% Saponin and 2.5% normal donkey serum. Secondary immunostaining was performed with Alexa Fluor® antibodies (ThermoFisher) used at 1μg/ml. Nuclei were identified using DAPI (100ng/ml; D8417, Sigma). Stained sections were imaged using the Operetta® High Content Imaging and Analysis system (PerkinElmer) and Harmony® software (PerkinElmer) for whole section images and a NanoZoomer S60 Digital slide scanner (Hamamatsu) for all other immunohistochemical imaging, unless otherwise noted.

To quantify MyRF, SOX10, OLIG2, CC1, or PDGFα positive cells, counts were performed along the length of the whole corpus callosum, the cerebellum, and the brainstem in medial sagittal sections from three animals per genotype. CC1 and OLIG2 or PDGFα and OLIG2 double-positive were determined from these counts. Counts were performed in a semi-automated manner using ImageJ (National Institutes of Health). To quantify GFAP and IBA1 staining, fluorescence intensity was measured using Adobe Photoshop along the length of the whole corpus callosum, the cerebellum, and the brainstem from medial sagittal sections from three animals per genotype. To quantify cleaved caspase 3 staining, sections from regions starting at the sagittal midline to 600 microns from the midline were used and cleaved caspase 3 positive cells were counted along the entire length of the corpus callosum, white matter of the cerebellum and entire brainstem to determine the total number of apoptotic cells per treatment group. All counts and quantifications were performed in a blinded manner. One-way ANOVA with Tukey correction and two-way unpaired t-tests, or a one-way ANOVA with Dunnett's correction for multiple comparisons were used to determine statistical significance across CRISPR or ASO cohorts, respectively.

qRT-PCR

Mice from CRISPR or ASO studies were euthanized using isoflurane overdose. Different brain regions (cerebral cortex, cerebellum, and brainstem) were harvested and flash frozen. Each region was split in two and half was used for RNA quantification using qRT-PCR, the other for western blot analysis (see below). TRI Reagent (R2050-1-200, Zymo Research) was separately added to tissue and samples were homogenized using Kontes Pellet Pestle Grinders (KT749520–0000, VWR). RNA was extracted using the RNeasy Mini Kit (74104, Qiagen) according to the manufacturer's instructions. Reverse transcription was performed using the iScript cDNA Synthesis Kit (1708891, Biorad) with 1μg of RNA per reaction. Real-Time PCR was then performed on an Applied Biosystems 7300 Real-time PCR system with 10ng cDNA per sample in quadruplicate using Taqman gene expression master mix (4369016, ThermoFisher) and the following pre-designed Taqman gene expression assays (4351370, ThermoFisher): *Plp1* (Mm01297210_m1), *Mbp* (Mm01266402_m1) and *Actb* (Mm00607939_s1) (endogenous control). Expression values were normalized to *Actb* and to wild-type samples (for CRISPR cohort) or wild-type untreated samples (for ASO-treated wild-type cohort). One-way ANOVA with Tukey correction and two-way unpaired t-tests, or a one-way ANOVA with Dunnett's correction for multiple comparisons were used to determine statistical significance across CRISPR or ASO cohorts, respectively.

Protein quantification and western blot

Tissues were obtained as described above. Protein lysis buffer consisting of RIPA buffer (R0278, Sigma), cOmplete™ Mini EDTA-free Protease Inhibitor Cocktail (11836170001, Sigma), Phosphatase Inhibitor Cocktail 3 (P0044, Sigma), Phosphatase Inhibitor Cocktail 2 (P5726, Sigma), and BGP-15 (B4813, Sigma) was added to each sample. Tissue was homogenized using Dounce Tissue Grinders (D8938, Sigma). Lysate was separated by centrifugation at 17000g for 15 minutes at 4°C. A BCA standard curve was generated using the Pierce BCA Protein Assay Kit (23225, Thermo Scientific) and used to samples to an equivalent protein concentration. Equal amounts of sample were run on a NuPAGE 4–12% Bis-Tris Protein gel (NP0335BOX or NP0329BOX, Thermo Fisher), then electrophoretically transferred to a PVDF membrane (LC2002, Invitrogen or 926–31097, Li-Cor). The membrane was blocked with 5% milk in TBS-T for an hour, then hybridized with mouse anti-MBP antibody (1μg/mL; 808401, Biolegend; RRID:AB_2564741) or rat anti-PLP antibody (1:1000; clone AA3, Lerner Research Institute Hybridoma Core, Cleveland, OH) overnight at 4°C. Blots were then washed in TBS-T and incubated in goat anti-mouse HRP (1:2500, 7076, Cell Signaling), goat anti-rat HRP (1:2500, 7077, Cell Signaling), or IRDye secondaries (1:20000, 925, Li-Cor). Each sample was normalized to B-actin using HRP-conjugated mouse anti-B-actin (1:10000, A3854, Sigma-Aldrich; RRID:AB_262011). All secondary antibodies were incubated for one hour at room temperature. Blots were analyzed with the Odyssey® Fc imaging system (Li-Cor). One-way ANOVA with Tukey correction and two-way unpaired t-tests, or a one-way ANOVA with Dunnett's correction for multiple comparisons were used to determine statistical significance across CRISPR or ASO cohorts, respectively. Raw annotated images of full western blots are provided in Supplementary Data 2 and 7.

Sample preparation for label-free expression discovery

Samples in protein lysis buffer were cleaned of detergent using a previously published filter-aided sample preparation protocol with a 10-kDa molecular weight cutoff filter (Millipore, Billerica, MA) and buffer exchanged with 8M Urea in 50mM Tris-pH-8.0 to a final volume of 50μL[40]. Proteins were reduced on filter with 10mM dithiothreitol (8M Urea, 50mM Tris-pH-8.0) for 1-hour at 37°C, followed by alkylation with 25mM iodoacetaminde (8M Urea, 50mM Tris-pH-8.0) for 30min in the dark. The 8M urea was then adjusted to 4M (50mM Tris-pH-8.0) and samples were concentrated to a final volume of 50μL. Next, 10μg of total protein were digested with lysyl endopeptidase (Wako Chemicals, Richmond, VA) at an enzyme:substrate ratio of 1:30 for 2-hours at 37°C. The urea concentration was then adjusted to 2M using 50mM Tris, pH 8, followed by an overnight trypsin digestion using sequencing grade trypsin (Promega, Madison, WI) at an enzyme:substrate ratio of 1:30 at 37°C.

Reverse phase LC-MS/MS analysis

Three hundred nanograms of each sample were analyzed by LC-MS/MS using a LTQ-Orbitrap Elite mass spectrometer (Thermo Scientific, San Jose, CA) equipped with a nanoAcquity™ Ultra-high pressure liquid chromatography system (Waters, Taunton, MA). The injection order on the LC-MS was randomized over all samples. Blank injections were

run after each sample to minimize carry-over between samples. Mobile phases were organic phase A (0.1% formic acid in water) and aqueous phase B (0.1% formic acid in acetonitrile). Peptides were loaded onto a nanoACQUITY UPLC® 2G-V/M C18 desalting trap column (180 μm × 20 mm nano column, 5 μm, 100 Å) at flow rate of 0.300μl/minute. Subsequently, peptides were resolved in a nanoACQUITY UPLC® BEH300 C18 reversed phase column (75μm × 250 mm nano column, 1.7μm, 100 Å; Waters, Milford, MA) followed by a gradient elution of 1–40 % of phase B over 240 minutes (isocratic at 1% B, 0–1 min; 2–42% B, 2–212 min; 42–90% B, 212–223 min; and 90–1% B, 223–240 min). A nano ES ion source at a flow rate of 300 nL/min, 1.5 kV spray voltage, and 270 °C capillary temperature was utilized to ionize peptides. Full scan MS spectra (m/z 380–1800) were acquired at a resolution of 60,000 followed by twenty data dependent MS/MS scans. LC-MS/MS raw data were acquired using the Xcalibur software (Thermo Fisher Scientific, version 2.2 SP1).

Data processing for protein identification and quantification

The LC-MS/MS raw files (one for each sample) were imported into PeaksStudio (BioinformaticsSolutions, Ontario, Canada) and processed as previously described[41,42]. A database was created that included PLP wild-type and predicted mutant isoforms. Search settings were as follow: trypsin enzyme specificity; mass accuracy window for precursor ion, 10 ppm; mass accuracy window for fragment ions, 0.8 Da; carbamidomethylation of cysteines as fixed modifications; oxidation of methionine as variable modification; and one missed cleavage. Peptide identification criteria were a mass accuracy of ≤10 ppm, and an estimated False Discovery Rate (FDR) of less than 2%. Normalization of signal intensities across samples was performed using the average signal intensities obtained in each sample. The fold change (FC) was then calculated using these average intensity values for the protein across the two samples.

Electron microscopy

Mice were anesthetized with isoflurane and tissue was collected after terminal transcardial perfusion with PBS followed by 4% paraformaldehyde and 2% glutaraldehyde (16216, Electron Microscopy Sciences) in 0.1M sodium cacodylate buffer, pH 7.4 (11652, Electron Microscopy Sciences), except for 6 month optic nerve samples which were placed directly into fixative without perfusion. Samples were post-fixed with 1% osmium tetroxide (19150, Electron Microscopy Sciences) and stained with 0.25% uranyl acetate (22400, Electron Microscopy Sciences), en bloc. Samples were dehydrated using increasing concentrations of ethanol, passed through propylene oxide, and embedded in Eponate 12™ epoxy resin (18012, Ted Pella). Silver–colored sections were prepared (Leica EM UC6), placed on 300 mesh nickel grids (T300-Ni, Electron Microscopy Sciences), stained with 2% uranyl acetate in 50 % methanol, and stained with lead citrate (17800, Electron Microscopy Sciences). Sections were imaged using a FEI Tecnai Spirit electron microscope at 80 kV. Myelinated axons were manually counted from the sections made on the middle portion of the optic nerve lengthwise, the medial portion of the genu for the corpus collosum, and corticospinal tracts at the pontine level of the brainstem. Three independent areas were counted for each region using Adobe Photoshop (Adobe Systems). Two-way unpaired t-tests or a one-way ANOVA with Dunnett's correction for multiple comparisons were used to determine statistical significance across CRISPR or ASO cohorts, respectively.

Optic nerve electrophysiology

Mice were deeply anesthetized with isoflurane and euthanized. Each eye with its attached optic nerve was dissected and placed in Tyrode's solution consisting of 129mM NaCl (BP358–212, Fisher Scientific), 3mM KCl (BP366–500, Fisher Scientific), 1.2mM NaH_2PO_4 (1–3818, J. T. Baker Chemical), 2.4mM $CaCl_2$ (C79–500, Fisher Scientific), 1.3mM $MgSO_4$ (M2643, Sigma), 20mM $NaHCO_3$ (S233–500, Fisher Scientific), 3mM HEPES (H3375, Sigma), 10mM glucose (G5767, Sigma), oxygenated using a 95%O_2/5% CO_2 gas mixture. Each nerve was carefully cleaned, transected behind the eye, at the optic chiasm, and allowed to recover for one hour in oxygenated Tyrode's solution at room temperature (22–24°C). Each end of the nerve was set in suction electrodes, pulled from polyethylene tubing (PE-190, BD Biosciences). Monophasic electrical stimuli were applied to the proximal end of the nerve and recordings were captured at the distal end. The recovery of the response was monitored every 20 min for one hour, and only fully recovered samples were subjected to additional stimuli. Stimuli were generated with a S48 stimulator (Grass Technologies) and isolated from ground with PSIU6B unit (Grass Technologies). Supra-threshold stimulus was determined using 30μs stimulus duration. The response was amplified 100X with P15D preamplifier (Grass Technologies), monitored with oscilloscope (V1585, Hitachi), digitized with Digidata1550A (Axon Instruments) and recorded using 50kHz sampling rate with AxoScope software (Axon Instruments). The distance between the electrodes was measured and used to calculate the conduction velocity of the compound action potential (CAP) peaks at their latency. Recorded signals were analyzed using AxoScope software. One-way ANOVA with Tukey correction and two-way unpaired t-tests, or a one-way t-test were used to determine statistical significance across CRISPR or ASO cohorts, respectively.

Open field testing

Locomotion was assessed by open field testing. Animals were placed in the center of a 20-inch by 20-inch square box and all movements were captured for a total of five minutes using ANY-maze software version 5.0 (Stoelting Co). Total distance traveled was reported for each animal. One-way ANOVA with Tukey correction and two-way unpaired t-tests, or a one-way ANOVA with Dunnett's correction for multiple comparisons were used to determine statistical significance across CRISPR or ASO cohorts, respectively.

Rotarod testing

Motor performance was assessed using a Rota Rod Rotomax 5 (Columbus Instruments) with a 3cm diameter rotating rod. Immediately prior to testing animals were trained at a constant speed of 4 rounds per minute (rpm) for a total of two minutes. Testing began at 4 rpm with an acceleration of 0.1 rpm/s. Time to fall was recorded from three independent trials, and the average value for each animal was reported. Animals were allowed to rest for at least five minutes between training and each experimental trial. Animals that failed training were assigned a value of 0 for all three trials for a particular timepoint. One-way ANOVA with Tukey correction and two-way unpaired t-tests, or a one-way ANOVA with Dunnett's correction for multiple comparisons were used to determine statistical significance across CRISPR or ASO cohorts, respectively.

Immunocytochemistry

Cells were fixed with 4% paraformaldehyde (PFA) in phosphate buffered saline (PBS). After fixation, cells were permeabilized with 0.2% Triton X-100 in PBS followed by blocking in 10% donkey serum in PBS. Cells were stained overnight at 4°C with the following primary antibodies diluted in blocking solution: mouse anti-MBP (1:500; 808401, Biolegend; RRID:AB_2564741), rat anti-PLP (1:5000; clone AA3, Lerner Research Institute Hybridoma Core, Cleveland, OH), goat anti-SOX10 (2μg/mL; AF2864, R&D Systems; RRID:AB_442208), rabbit anti-OLIG2 (1:1000; 13999–1-AP, ProteinTech; RRID:AB_2157541), rabbit anti-NANOG (0.4μg/mL; AB21624, Abcam; RRID:AB_446437), mouse anti-OCT3/4 (0.4μg/mL; SC-5279, Santa Cruz; RRID:AB_628051). For secondary immunostaining, Alexa Fluor® antibodies (ThermoFisher) were used at 1μg/ml, and DAPI (100ng/mL) was employed to identify nuclei. Images were captured using Leica DMi8 fluorescence microscope (iPSCs) or Operetta® High Content Imaging and Analysis system and Harmony® software (OPCs and oligodendroctytes), the latter quantified using Columbus software (PerkinElmer).

Generation of iPSCs

Tail tips (2 mm piece from 8 day old CR-*impy* mice) were bisected, placed on Nunclon-Δ 12-well plates (150628, ThermoFisher), and covered with a circular glass coverslip (12-545-102; Fisher Scientific) to maintain tissue contact with the plate and enable fibroblast outgrowth. Tail-tip fibroblasts were cultured in ‘fibroblast medium’ consisting of DMEM (11960069, ThermoFisher) with 10% fetal bovine serum (FBS; 16000044, ThermoFisher), 1x non-essential amino acids (11140050, ThermoFisher), 1x Glutamax (35050061, ThermoFisher), and 0.1 mM 2-mercaptoethanol (M3148, Sigma Aldrich) supplemented with 100U/mL penicillin-streptomycin (15070–063, ThermoFisher). Medium was changed every day for the first 3 days and then every other day.

Fibroblasts were seeded at approximately 1.4×10^4 cells/cm^2 on Nunclon-Δ dishes in fibroblast medium, and allowed to equilibrate overnight. The following day medium was removed and replaced with an equal volume of pHAGE2-TetOminiCMV-STEMCCA-W-loxp lentivirus encoding a floxed, doxycycline-inducible polycistronic Oct4, Sox2, Klf4, and c-Myc construct and pLVX-Tet-On-Puro (632162, Clontech) lentivirus supplemented with 8μg/mL polybrene (107689, Sigma). Lentivirus was prepared using the Lenti-X Packaging Single Shots (631275, Clontech) according to manufacturer’s instructions. Three hours later lentivirus medium was removed and replaced with fibroblast medium supplemented with 2 μg/ml doxycycline (631311, Clontech). The following day media was removed and replaced with an equal volume of pHAGE2-TetOminiCMV-STEMCCA-Wloxp and pLVX-Tet-On-Puro lentivirus supplemented with 8μg/mL polybrene. Three hours later lentivirus media was diluted 1:2 with fibroblast medium. Medium was changed each day with fibroblast medium supplemented with 2 μg/ml doxycycline and 10^3 units/ml LIF. After 3 days fibroblasts were lifted using Accutase and seeded on Nunclon-Δ plates, atop a feeder layer of irradiated mouse embryonic fibroblasts (iMEFs; produced in-house) previously plated at 1.7×10^4 cells/cm^2 on 0.1% gelatin (1890, Sigma) coated Nunclon-Δ plates in “pluripotency medium” consisting of Knockout DMEM (10829–018, ThermoFisher), 5% FBS, 15% knockout replacement serum (10828028, ThermoFisher), 1x Glutamax, 1x nonessential

amino acids, 0.1 mM 2-mercaptoethanol, and 10^3 units/ml LIF (LIF; ESG1107, EMD Millipore) supplemented with 2 μg/ml doxycycline. Medium was changed every day until iPSC colonies began to emerge. Individual colonies were picked and dissociated in Accutase and were individually plated in single wells of Nunclon-Δ 12-well plates, atop an iMEF feeder layer in pluripotency medium supplemented with 2 μg/ml doxycycline. Clones were further expanded, with daily medium changes. iPSC colonies were stained for pluripotency markers Nanog and Oct4 and karyotyped at the seventh passage after derivation (Cell Line Genetics; Madison, WI). CR-*impy* iPSCs were derived and characterized for this study (line identifier jpCR100.1). Isogenic comparator *jimpy* (line identifier i.jp-1.6) and wild-type (line identifier i.wt-1.0) iPSC lines were described and characterized separately[14]. All cell cultures in the laboratory are routinely tested for mycoplasma contamination with consistently negative results. Genotypes of iPSCs were re-verified prior to use. For characterization iPSCs were immunostained for NANOG and OCT3/4, and counterstained with DAPI.

Generation of iPSC-derived OPCs

iPSCs were differentiated to OPCs as previously described[43,44]. In brief, iPSCs were isolated from their iMEF feeder layer using 1.5mg/mL collagenase type IV (17104019, ThermoFisher) and dissociated with either 0.25% Typsin-EDTA or Accutase and seeded at 7.8×10^4 cells/cm2 on Costar Ultra-Low attachment 6-well plates (3471, Corning). Cultures were then directed through a stepwise differentiation process to generate pure populations of OPCs. OPCs were maintained in “OPC medium” consisting of DMEM/F12 (11320082, ThermoFisher), 1x N2 supplement (AR009, R&D Systems), 1x B-27 without vitamin A supplement (12587–010, ThermoFisher), and 1x Glutamax (collectively “N2B27 medium”), supplemented with 20 ng/mL fibroblast growth factor 2 (FGF2; 233-FB, R&D Systems) and 20 ng/mL platelet-derived growth factor-AA (PDGF-AA; 221-AA, R&D Systems). Medium was changed every other day. All cell cultures in the laboratory are routinely tested for mycoplasma contamination with consistently negative results. For characterization of purity, iPSC-derived OPCs were fixed with 4% PFA and immunostained for canonical OPC transcription factors, OLIG2 and SOX10, and counterstained with DAPI.

In vitro assessment of oligodendrocyte differentiation from OPCs

OPCs from each genotype were plated in parallel onto Nunclon-Δ 96-well plates (150628, ThermoFisher) that were first coated with 100 μg/mL poly(L-ornithine) (P3655, Sigma), followed by 10 μg/ml laminin solution (L2020, Sigma). For the oligodendrocyte differentiation assay, 25,000 cells were seeded per well in media that consisted of DMEM/F12 (11320082, ThermoFisher), 1x N2 supplement (AR009, R&D Systems), 1x B-27 without vitamin A supplement (12587–010, ThermoFisher), and 1x Glutamax, supplemented with T3 (40ng/ml), Noggin (100ng/ml), cAMP (10μM), IGF (100ng/ml) and NT3 (10ng/ml). All plates were incubated at 37°C and 5% CO_2 for 3 days. Cells were fixed and immunostained for MBP and PLP, and counterstained with DAPI. All quantifications were normalized to initial cell counts at plating.

Assessment of gene expression modulation in the oligodendrocyte lineage by *Hdac2*-targeting ASOs

Two ASOs were designed to target mouse *Hdac2*. ASO-*Hdac2*.a consisted of a 20-mer nucleotide sequence (5′- CTCACTTTTCGAGGTTCCTA-3′) with 2′-O-methoxyethyl (MOE) modifications and a mixed backbone of phosphorothioate and phosphodiester internucelotide linkages. ASO-*Hdac2*.b consisted of a 16-mer nucleotide sequence (5′-CATCATCTATACCATC-3′) with 2'-O-ethyl (cEt) modifications with a full backbone of phosphorothioate internucelotide linkages. To determine if ASOs could reduce effectively target oligodendrocyte linage cells and reduce gene expression, we administered *Hdac2*-targeting ASOs to 8 week old C57BL/6J mice (Jackson Labs) via single 300μg ICV injection. After 2 weeks mice were sacrificed and processed for histology. Formalin-fixed, paraffin embedded brain and spinal cord sections were stained for NG2 to label OPCs in the study dosed with *Hdac2*.a ASO, and APC/CC1 to oligodendrocytes in the study dosed with *Hdac2*.b ASO, as well for HDAC2 to examine ASO-mediated knockdown of this target. Images were captured using an epifluorescent imaging system (EVOS, ThermoFisher Scientific).

Plp1-targeting ASO design and characterization

Second generation ASOs were designed to target mouse *Plp1*. ASOs consisted of 20-mer nucleotide sequences with 2′-O-methoxyethyl (MOE) modifications and a mixed backbone of phosphorothioate and phosphodiester internucelotide linkages. ASOs were screened for efficacy in primary E16 cortical cultures, as previously described[45]. Briefly, cells were treated with ASOs at 37°C/5% CO2 for 3 days, RNA was isolated, and *Plp1* transcript level was quantified with qRT-PCR on Step One instruments (Thermo Fisher). *Plp1* mRNA was normalized to total RNA measured with the Quant-iTTM RiboGreen® RNA reagent. ASOs that efficiently reduced *Plpl* mRNA were selected for *in vivo* screening and tolerability studies.

Lead ASOs were administered to 8 week old C57BL/6J mice via single 500μg ICV injection and *Plp1* mRNA levels were measured by qRT-PCR in cortex and spinal cord tissue after 2 weeks. ASOs with greater than 90% *Plp1* mRNA reduction were selected for further characterization. Selected ASOs were administered to mice via single 300μg ICV bolus injection to test for efficacy and tolerability, as measured by markers of glial cell activation, 8 weeks post-ICV injection. Levels of *Plp1* mRNA as well as markers of astrocytes, microglia, and monocytes (*Gfap*, *Aif1*, and *CD68, respectively*) were assessed by qRT-PCR using the custom primer and probe sets (Integrated DNA Technologies) listed in Supplementary Table 4.

Immunohistochemical staining was used to assess morphology of astrocytes, microglia, and oligodendrocyte using anti-GFAP, IBA1 (DAKO), and MBP (Abcam) antibodies, respectively, in formalin-fixed, paraffin embedded brain and spinal cord sections. *Plp1* ASO.a (intron 5) and ASO.b (3' UTR) were selected for use in *jimpy* mice, as well as a control ASO with no known murine target. ASO sequences were as follows:

ASO control: 5′- CCTATAGGACTATCCAGGAA-3′

ASO *Plp1*.a: 5′-GCTCATTGATTCAAGTACAT-3′

ASO *Plp1*.b, 5′-GCATTTACCCGAAGGCCATT-3′

Each *Plp1*-targeting ASO was further evaluated for potential off-target effects. Bowtie aligner [58] was used to identify putative ASO off-target transcript sequences, with up to three base mismatches. This analysis identified potential off-target sequence in *Xylt1* for ASO *Plp1*.a and *Scfd1* and *Tpk1* for ASO *Plp1*.b, each having exactly two mismatches. To determine if these transcripts were targeted by *Plp1* ASO.a or ASO.b, adult mice (8 weeks of age, C57Bl6/J) were administered 30, 100, or 300μg of each ASO by ICV injection. After two weeks spinal cord tissues were collected and levels of *Xylt1*, *Scfd1*, and *Tpk1* were measured by qRT-PCR using the custom primer and probe sets (Integrated DNA Technologies) listed in Supplementary Table 4.

Optimum therapeutic dosage for use in early postnatal injection was determined by injecting wild-type C57BL/6J mice pups at postnatal day 1 using three different doses (10, 30, or 60 μg) of ASO *Plp1*.a or ASO *Plp1*.b, along with a control non-targeting ASO. Mice were sacrificed three weeks later and analyzed by for levels of *Plp1* mRNA in the spinal cord using qRT-PCR. One-way ANOVA with Dunnett's correction for multiple comparisons was used to determine statistical significance across treatments.

Therapeutic application of ASOs to postnatal mice

Male pups from crosses between *jimpy* mutation carrier females and wild-type males were administered 30μg of either *Plp1*-targeting ASOs *Plp1*.a, *Plp1*.b, a control non-targeting ASO, or left untreated. ASOs were administered using a Hamilton 1700 gastight syringe (7653–01, Hamilton Company) by ICV injection to cryoanesthetized mice. The needle was placed between bregma and the eye, 2/5 the distance from bregma, and inserted to a depth of 2mm[46]. A total volume of 2μl was administered to the left ventricle. Mice were allowed to recover on a heating pad and subsequently reintroduced to the dam. Injections were performed with the investigator blinded to the genotype.

Mice were genotyped during the first postnatal week and monitored daily for onset of typical *jimpy* phenotypes including tremors, seizures, and early death by 3 weeks of age. Lifespan was determined for each animal with statistical significance among groups determined using the log-rank test. All mice surviving to a pre-determined endpoint of 8 months of age were sacrificed for histological analysis. Additionally, animals were analyzed using rotarod, open field, and optic nerve electrophysiology. Details and metadata for all mice in this study are found in Supplementary Data 6.

Evaluation of respiration

At postnatal day 19 or 20, male pups were placed in a plethysmograph chamber and pressure changes caused by animal respiration were measured using a differential pressure transducer (Emka). The data collection was started when the mice were placed in the chamber and continuously recorded at 1 KHz sampling rate. After placing the mice in the chamber, it was first flushed with normal air (79% nitrogen, 21% oxygen) over a 1 hour period to acclimate the mice and determine basal breathing activity. The chamber was then flushed with

hypercapnic gas (74% nitrogen, 21% oxygen, 5% carbon dioxide) for 15 minutes and the data collected over the subsequent 15–30 minute period was used for analysis. Next, the chamber was flushed with normal air for 15 minutes. Hypoxic gas (89.5% nitrogen, 10.5% oxygen) was then introduced to the chamber over 10 minutes, with the data collected over this period used for analysis. After the hypoxic gas challenge mice were weighed and sacrificed. Gas flow rate over the entire experiment was 0.75L/min per chamber. Recorded breaths lasting for at least 20 seconds, continuously, and marked with a 100% success rate using IOX2 software (Emka) were used for subsequent data analysis for the normal air and hypercapnic conditions. Recorded breaths in the hypoxic condition were not continuous for more than 20 seconds so only breaths marked with a 100% success rate in the IOX2 software were used for further data analysis. Survival during hypoxic challenge was determined for each animal with statistical significance among groups determined using the log-rank test. Variability of respiration was determined with statistical significance among groups determined using the Brown and Forsythe's test.

Reporting summary

Further information on research design is available in the Nature Research Reporting Summary linked to this paper.

Data availability

All data generated or analyzed during this study are included in this article and its supplementary information files. Source data for animal survival cohorts in Figs. 1b, k–l, and 3b, 4a–b are provided in Supplementary Data 1 and 6. Raw annotated western blot images for Extended Data Fig. 2b, d and Extended Data Fig. 7a, c are provided as Supplementary Data 2 and 7. Source data for all graphs are provided as separate Excel files. Animals and iPSC lines are available from P.J.T. upon request.

Extended Data

Extended Data Fig. 1 |. CRISPR nuclease induction of *Plp1* frameshift mutations in *jimpy* with high accuracy.

a, Annotated Sanger sequencing traces of wild-type, *jimpy*, and CR-*impy* mice showing the complex, frameshift in *Plp1* exon 3 from dual cutting of CRISPR/spCas9 sgRNAs in CR-*impy* mice as well as the *jimpy* point mutation in intron 4. sgRNA 3 and 7 sequences outlined by black boxes with the predicted double strand break site shown a black arrow. **b**, Table showing the top predicted on- and off-target sites for sgRNAs 3 and 7. CRISPR-induced indels were detected by whole genome sequencing of the CR-*impy* founder and three independent CR-*impy* F2 generation males, and consisted of an on-target 80bp

complex deletion (CR-*impy* deletion) in exon 3 of *Plp1* (green), an off-target 1 bp insertion in chromosome 6 (red), and an off-target 1 bp insertion in chromosome 11 (yellow). **c-e**, Integrative Genomics Viewer browser images showing aligned reads for the CR-*impy* founder, the *jimpy* control, and three CR-*impy* F2 males along with the detected indels at the on-target locus at exon 3 of *Plp1* on chromosome X (**c**), and off-targets on chromosome 6 (**d**) and chromosome 11 (**e**) depicted by the dashed green, red, and yellow boxes, respectively. sgRNA 3 or sgRNA 7 targeted sequences are depicted by black bars.

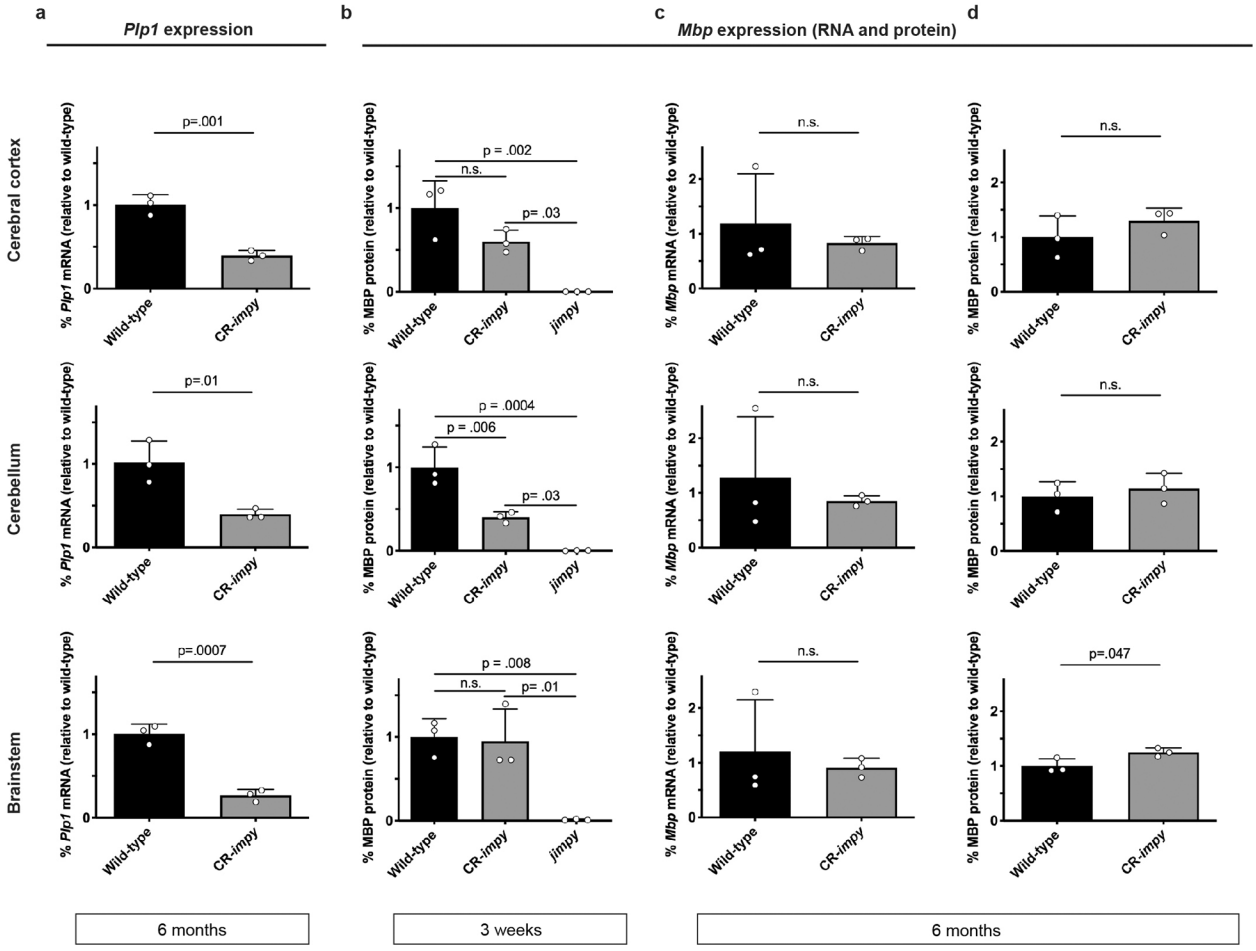

Extended Data Fig. 2 |. CRISPR-mediated suppression of *Plp1* in *jimpy* mice increases *Mbp* expression across multiple CNS regions.

a, RT-qPCR data showing the levels of *Plp1* transcript at 6 months (n=3 mice). **b**, Western blot data demonstrating the levels of MBP protein at 3 weeks (n=3 mice). **c**, RT-qPCR data showing the levels of *Mbp* transcript at 6 months (n=3 mice). **d**, Western blot data demonstrating the levels of MBP protein at 6 months (n=3 mice).

Individual data points represent the mean value of 4 technical replicates for each biological replicate (**a, c**) or independent biological replicates (**b, d**). Biological replicates (individual mice) indicated by open circles. Graph bars indicate mean ± standard deviation. p-values calculated using one-way ANOVA with Tukey correction at 3 weeks or two-way, an

unpaired two-sided t-test at later time points. p-values stated for p<0.1, otherwise not significant (n.s). See Supplementary Data 2 for full western blot images for all samples.

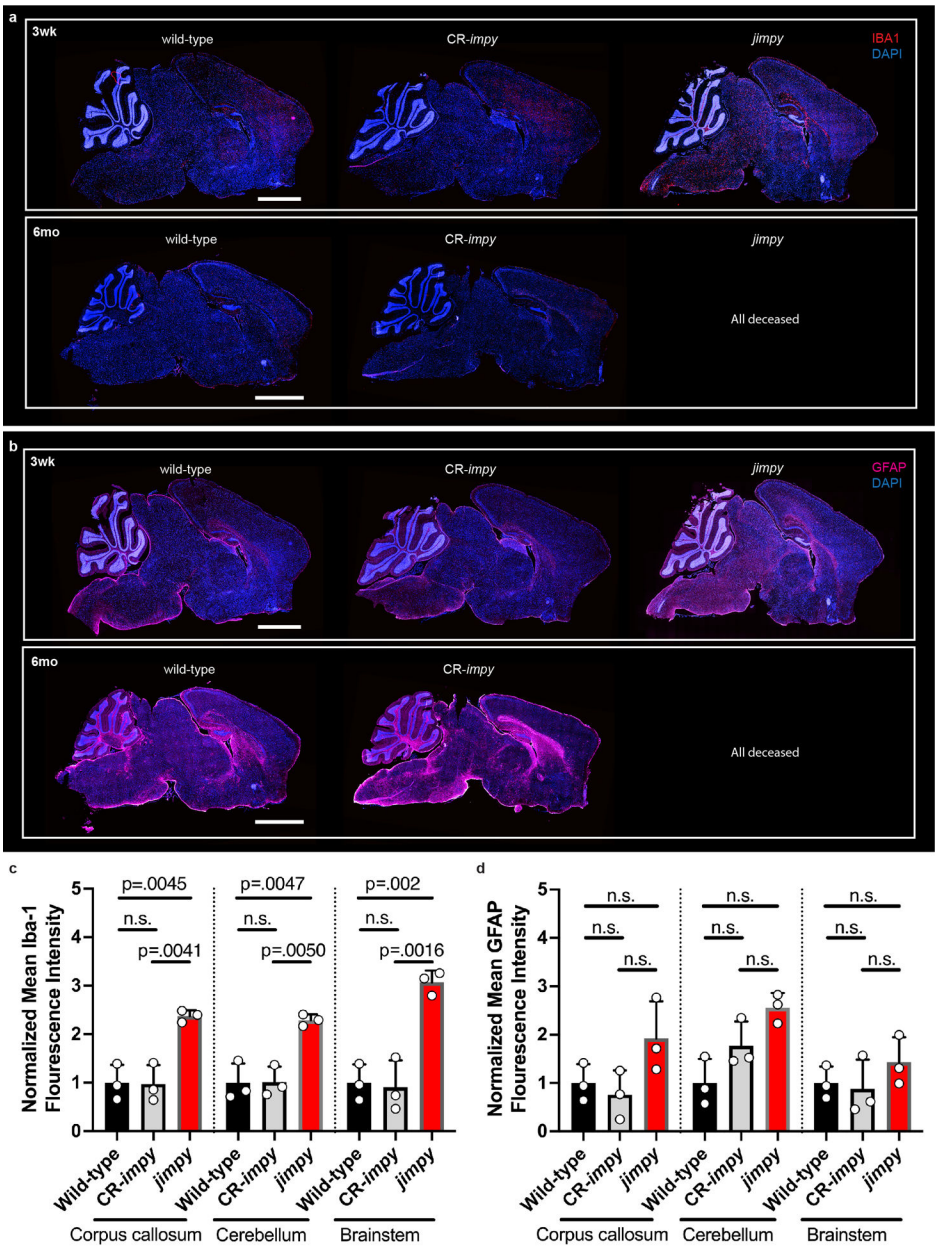

Extended Data Fig. 3 |. CRISPR-mediated suppression of *Plp1* in *jimpy* mice reduces markers of activated microglia and astrocytes

. a, Immunohistochemical images of whole-brain sagittal sections showing Iba1$^+$ microglia (red) and DAPI$^+$ nuclei (blue) across genotypes. Scale bar, 2mm. **b**, Immunohistochemical images of whole-brain sagittal sections showing GFAP$^+$ astrocytes (red) and DAPI$^+$ nuclei (blue) staining across genotypes. Scale bar, 2mm. **c-d**, Normalized mean signal intensity of (**c**) Iba1$^+$ microglia and (**d**) GFAP$^+$ astrocytes across genotypes and CNS regions (n=3 mice).

Biological replicates (individual mice) indicated by open circles. Graph bars indicate mean ± standard deviation. p-values calculated using one-way ANOVA with Tukey correction. p-values stated for p<0.1, otherwise not significant (n.s). See Supplementary Data 3–5 for representative source images of Iba-1 and GFAP staining.

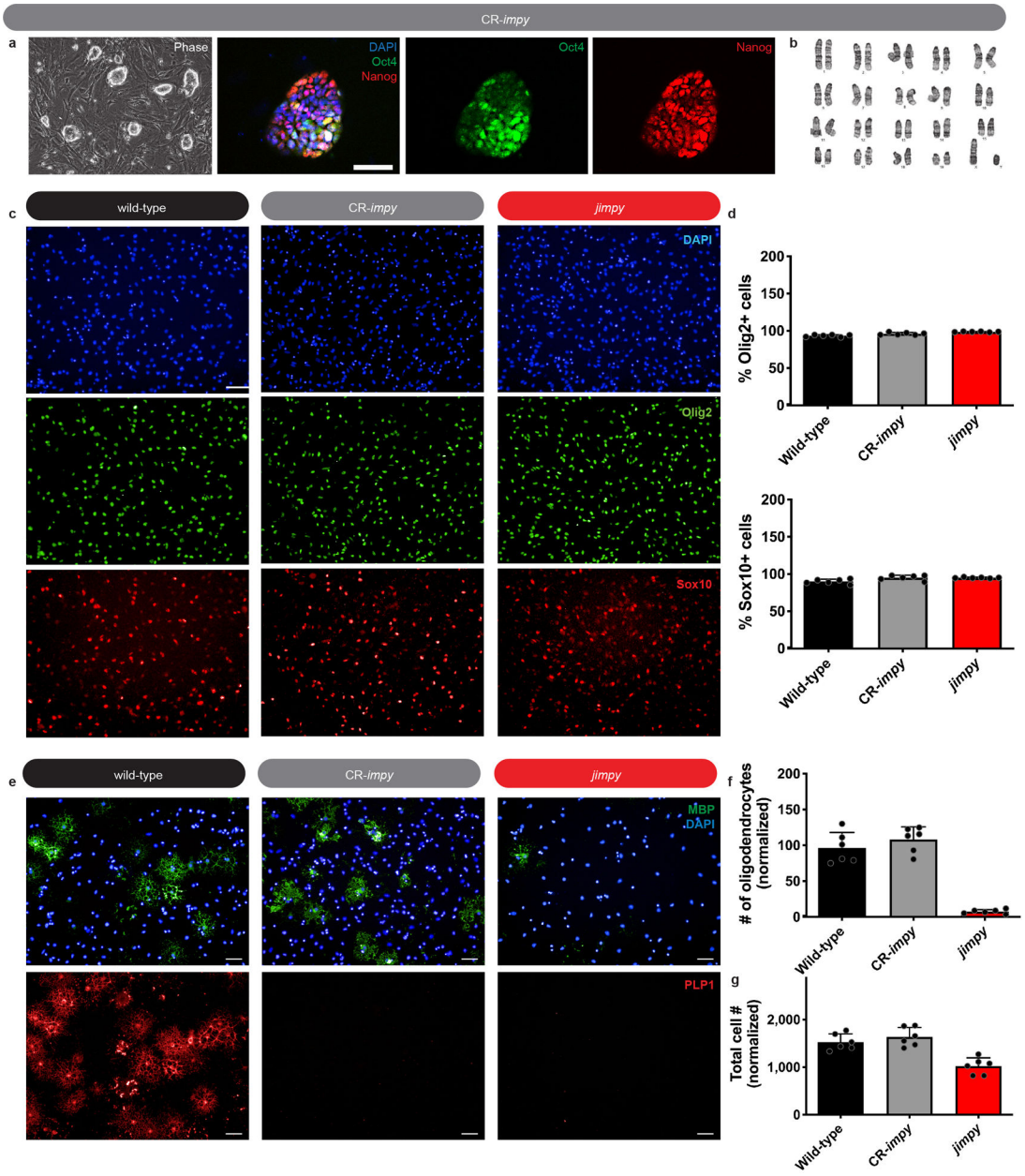

Extended Data Fig. 4 |. *Plp1* suppression in *jimpy* OPCs rescues survival of differentiating oligodendrocytes *in vitro*.

a, Phase and immunocytochemistry images of Oct4$^+$ and Nanog$^+$ iPSCs, along with DAPI$^+$ nuclei and **b**, normal karyotype of a CR-*jimpy* iPSC line used to generate OPCs. Scale bar, 50μm. **c**, Immunocytochemistry images showing Olig2$^+$ and Sox10$^+$ cells in OPC cultures, along with DAPI$^+$ nuclei, derived from iPSCs. Scale bar, 100μm. **d**, Percentage of Sox10$^+$

and Olig2^{+} cells in OPC cultures. **e**, Immunocytochemistry images of MBP^{+} and PLP^{+} oligodendrocytes. **f-g**, Quantification of (**f**) MBP^{+} oligodendrocytes and (**g**) total cell number (DAPI^{+} nuclei) from iPSC-derived OPCs differentiated *in vitro* for 3 days. Scale bar, 50μm.

Technical replicates (individual wells) for a single cell line per genotype indicated by black circles. Graph bars indicate mean ± standard deviation.

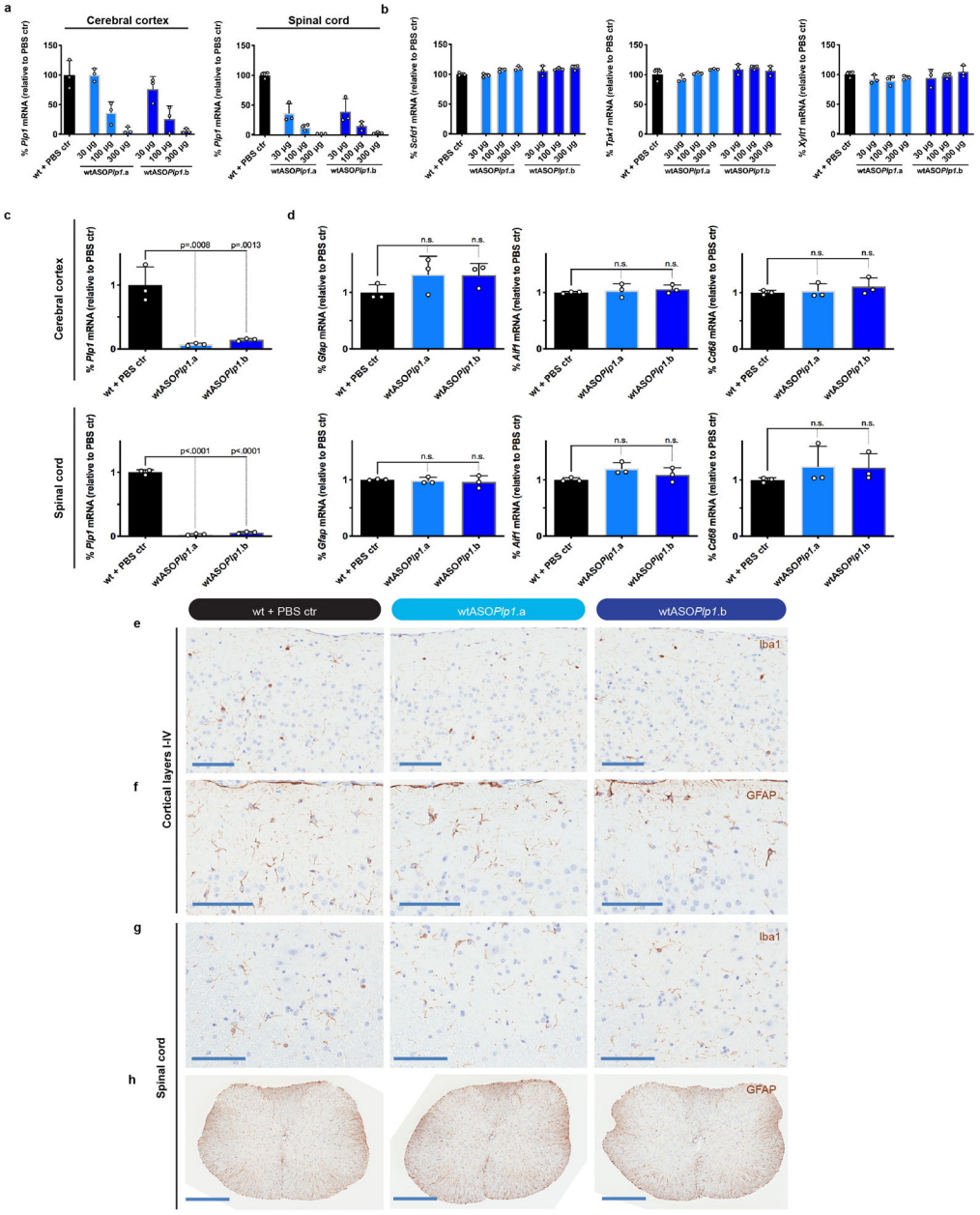

Extended Data Fig. 5 |. *Plp1*-targeted ASOs do not suppress off-target transcripts or activate glial cells.

a-b, RT-qPCR data showing the level of (a) *Plp1* transcript levels or (b) expression levels of off-target transcripts (up to 3 base mismatches) in the spinal cord for *Plp1*-tageting ASOs,

including *Xylt1* (off-target for ASO *Plp1*.a), *Scfd1*, or *Tpk1* (off-targets for ASO *Plp1*.b), 2 weeks post-injection of *Plp1*-targeting ASOs (30μg, 100μg, and 300μg doses) or PBS control in 8 week old adult wild-type (wt) mice (n=3 mice). **c-d**, RT-qPCR data showing *Plp1* transcript levels or tolerability by expression levels of *Gfap, Aif1*, and *Cd68* transcripts in the cerebral cortex and spinal cord, 8 weeks post-injection with the indicated ASOs (300μg dose) or PBS control in 8 week old wild-type mice (n=3 mice). **e-h**, Immunohistochemistry images with hematoxylin counterstain showing $Iba1^+$ or $GFAP^+$ astrocytes in (**e**) Cortical layers I-IV (Iba1), (**f**) cortical layers I-III (GFAP), (**g**) spinal cord dorsal horn grey/white matter intersection (Iba1), and (**h**) spinal cord (GFAP), 8 weeks post-injection with the indicated ASOs (300μg dose) or PBS control in 8 week old wild-type mice. Scale bar, 500μm.

Biological replicates (individual mice) indicated by open circles, representing the mean value of 3 technical replicates. Graph bars indicate mean ± standard deviation. p-values calculated using one-way ANOVA with Dunnett's correction for multiple comparisons. p-values stated for $p<0.1$, otherwise not significant (n.s).

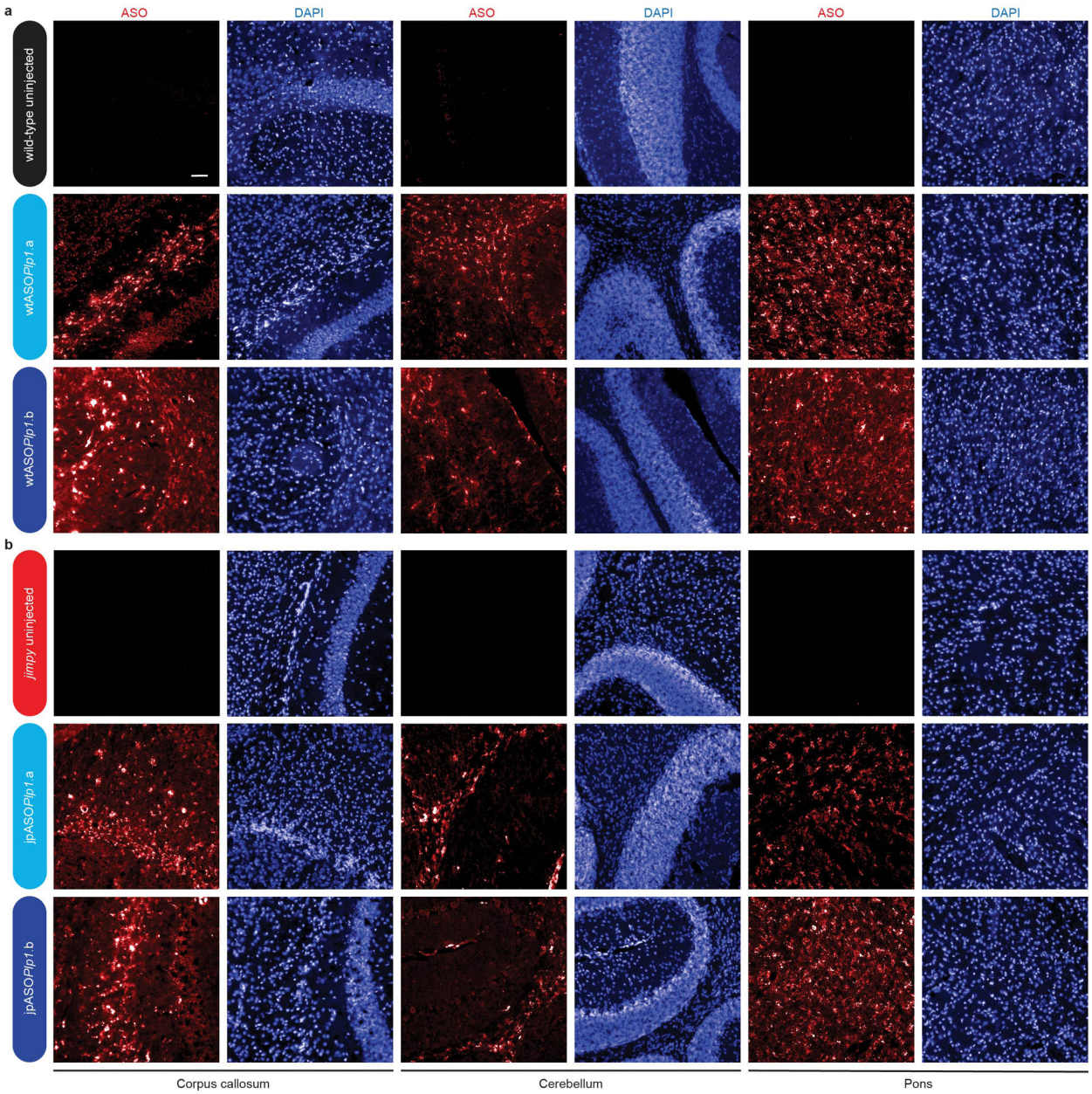

Extended Data Fig. 6 |. *Plp1*-targeted ASOs distribute widely throughout the CNS after ICV injection in postnatal mice.

a-b, Immunohistochemical images of brain sagittal sections showing ASO^{+} staining and DAPI^{+} nuclei (blue) of (**a**) wtASO*Plp1.a*, wtASO*Plp1.b*, and wild-type uninjected or (**b**) jpASO*Plp1.a*, jpASO*Plp1.b*, and uninjected *jimpy* mice, 3 weeks post-ASO injection (30μg dose at birth). Scale bar, 50μm.

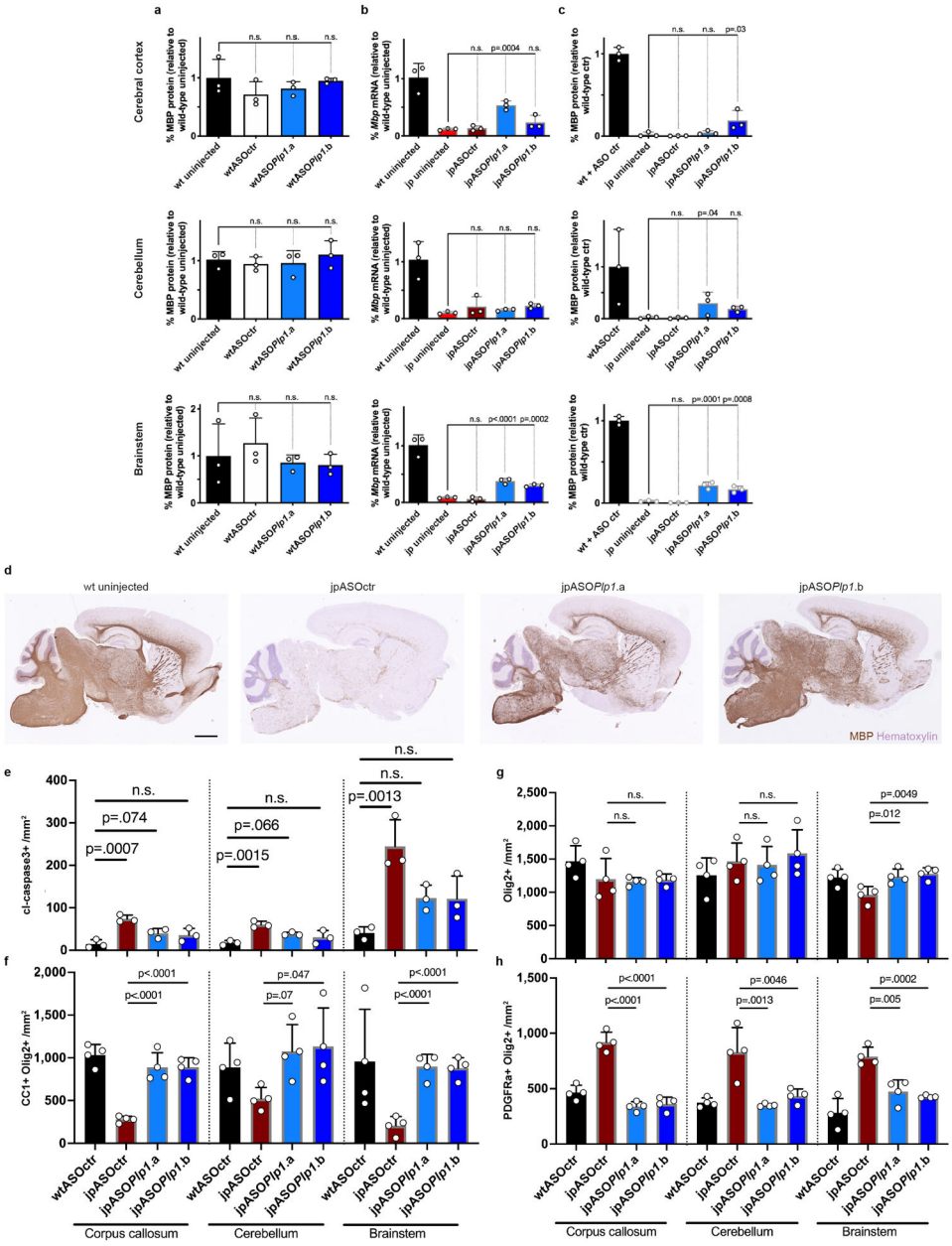

Extended Data Fig. 7 |. *Plp1*-targeting ASOs increase *Mbp* expression and rescue oligodendrocyte numbers in *jimpy* mice.

a, Western blot data showing the level of MBP protein (n=3 mice). **b**, RT-qPCR data showing the level of *Mbp* transcript (n=3 mice). **c**, Western blot data showing the level of MBP (n=3 mice). **d**, Immunohistochemistry images with hematoxylin counterstain of whole brain sagittal sections showing MBP$^+$ myelin. Scale bar, 1mm. **e**, Quantification of cleaved-caspase 3$^+$ apoptotic cells (n=3 mice). **f**, Quantification of CC1$^+$/Olig2$^+$ oligodendrocytes (n=4 mice). **g**, Quantification of the number of Olig2$^+$ glial lineage cells (n=4 mice). **h**, Quantification of the number of PDGFRα$^+$/Olig2$^+$ OPCs (n=4 mice).

All data collected at 3 weeks post-ASO injection (30μg dose at birth). Individual data points represent the mean value of 4 technical replicates for each biological replicate (individual

mice) (**b**) or independent biological replicates (individual mice) (**a, c-h**), indicated by open circles. Graph bars indicate mean ± standard deviation. p-values calculated using one-way ANOVA with Dunnett's correction for multiple comparisons. p-values stated for p<0.1, otherwise not significant (n.s). See Supplementary Data 4 for full western blot images for all samples.

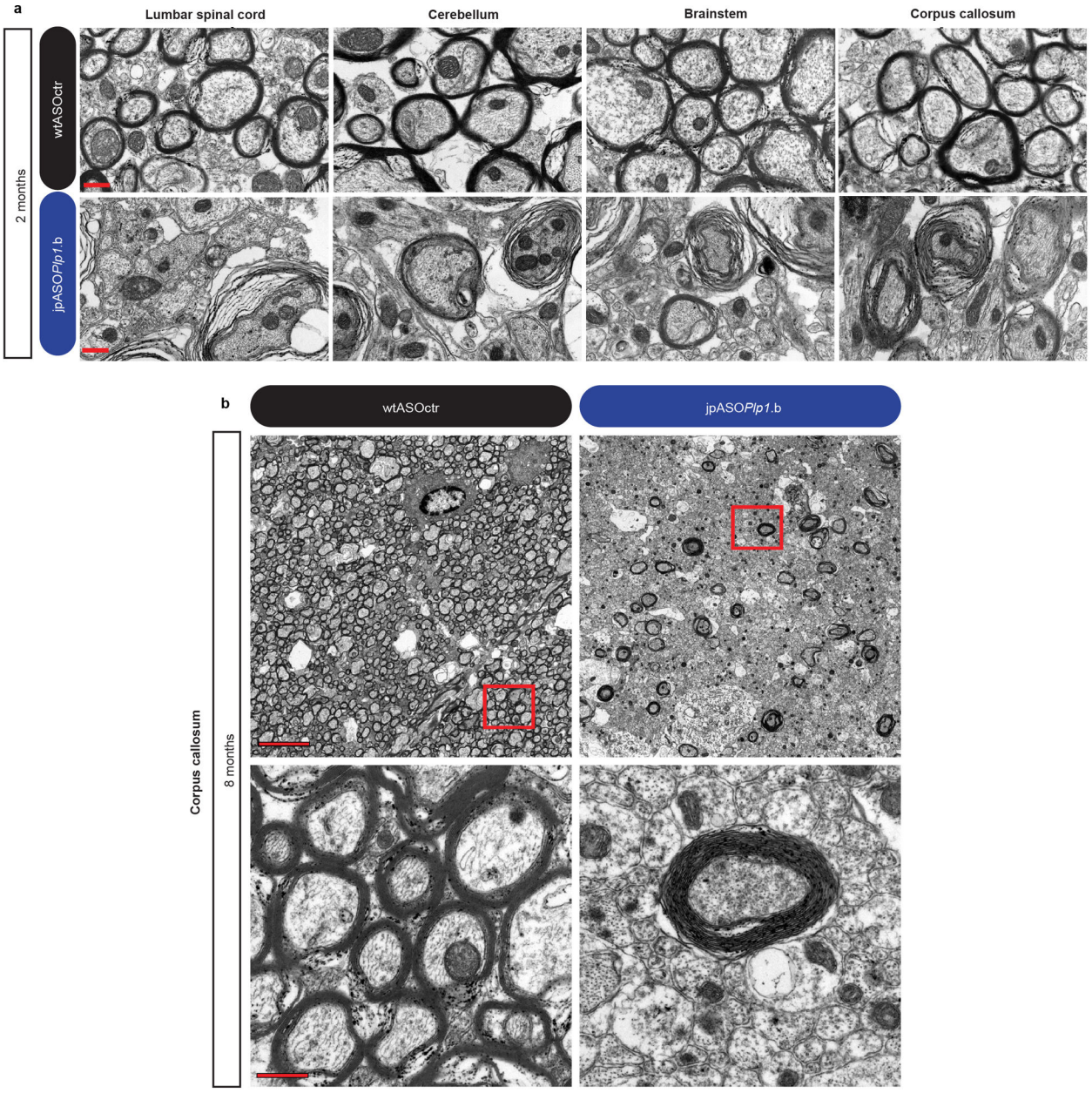

Extended Data Fig. 8 |. *Plp1*-targeted ASOs induce sustained myelination throughout the neuraxis in *jimpy* mice.

a-b, Electron micrograph images showing myelination of wtASOctr or jpASO*Plp1.b* at (**a**) 2 months and (**b**) 8 months. For a, scale bar, 0.5μm. For b, lower panel is a higher

magnification of red boxed area in the upper panel. Upper panel scale bar, 5μm and lower panel scale bar, 0.5μm.

Supplementary Material

Refer to Web version on PubMed Central for supplementary material.

Acknowledgments

This research was supported, in part, by grants from the NIH R01NS093357 (P.J.T.), T32GM007250 (M.S.E, Z.S.N., K.C.A), F30HD084167 (Z.S.N.), F30HD096784 (K.C.A.), and T32NS077888 (K.C.A.); the New York Stem Cell Foundation (P.J.T); the European Leukodystrophy Association (P.J.T.); and philanthropic contributions from the Research Institute for Children's Health and the Geller, Goodman, Fakhouri, Long, Matreyak, Peterson, and Weidenthal families. Additional support was provided by the Genomics, Small Molecule Drug Development, Transgenic, and Rodent Behavioral core facilities of the Case Western Reserve University (CWRU) Comprehensive Cancer Center (P30CA043703), the Data Analytics Core of the Department of Population and Quantitative Health Sciences at CWRU, the CWRU Light Microscopy Imaging Center (S10OD016164), the electron microscopy division of the Cleveland Clinic Lerner Research Institute Imaging Core, and the University of Chicago Genomics Facility. We are grateful to Lynn Landmesser, Peter MacFarlane, Robert Miller, Peter Scacheri, Tony Wynshaw-Boris, Ben Clayton, Simone Edelheit, Alex Miron, Hiroyuki Arakawa, Polyxeni Philippidou, Alicia Vagnozzi, Lucille Hu, Erin Cohn, Marissa Scavuzzo, Chris Allan, and Jared Cregg for technical assistance, discussion, and review of the manuscript.

References

1. Inoue K Pelizaeus-Merzbacher Disease: Molecular and Cellular Pathologies and Associated Phenotypes. Adv Exp Med Biol 1190, 201–216, doi:10.1007/978-981-32-9636-7_13 (2019). [PubMed: 31760646]
2. Wolf NI, van Spaendonk RML, Hobson GM & Kamholz J in GeneReviews((R)) (eds Adam MP et al.) (1993).
3. Garbern JY et al. Patients lacking the major CNS myelin protein, proteolipid protein 1, develop length-dependent axonal degeneration in the absence of demyelination and inflammation. Brain 125, 551–561 (2002). [PubMed: 11872612]
4. Griffiths I et al. Axonal swellings and degeneration in mice lacking the major proteolipid of myelin. Science 280, 1610–1613 (1998). [PubMed: 9616125]
5. Klugmann M et al. Assembly of CNS myelin in the absence of proteolipid protein. Neuron 18, 59–70 (1997). [PubMed: 9010205]
6. Goldman SA, Nedergaard M & Windrem MS Glial progenitor cell-based treatment and modeling of neurological disease. Science 338, 491–495, doi:10.1126/science.1218071 (2012). [PubMed: 23112326]
7. Gupta N et al. Neural stem cell engraftment and myelination in the human brain. Sci Transl Med 4, 155ra137, doi:10.1126/scitranslmed.3004373 (2012).
8. Saher G et al. Therapy of Pelizaeus-Merzbacher disease in mice by feeding a cholesterol-enriched diet. Nat Med 18, 1130–1135, doi:10.1038/nm.2833 (2012). [PubMed: 22706386]
9. Wishnew J et al. Umbilical cord blood transplantation to treat Pelizaeus-Merzbacher Disease in 2 young boys. Pediatrics 134, e1451–1457, doi:10.1542/peds.2013-3604 (2014). [PubMed: 25287453]
10. Tantzer S, Sperle K, Kenaley K, Taube J & Hobson GM Morpholino Antisense Oligomers as a Potential Therapeutic Option for the Correction of Alternative Splicing in PMD, SPG2, and HEMS. Mol Ther Nucleic Acids 12, 420–432, doi:10.1016/j.omtn.2018.05.019 (2018). [PubMed: 30195779]
11. Li H et al. Gene suppressing therapy for Pelizaeus-Merzbacher disease using artificial microRNA. JCI Insight 4, doi:10.1172/jci.insight.125052 (2019).

12. Nobuta H et al. Oligodendrocyte Death in Pelizaeus-Merzbacher Disease Is Rescued by Iron Chelation. Cell Stem Cell 25, 531–541 e536, doi:10.1016/j.stem.2019.09.003 (2019). [PubMed: 31585094]
13. Gruenenfelder FI et al. Neural stem cells restore myelin in a demyelinating model of Pelizaeus-Merzbacher disease. Brain 143, 1383–1399, doi:10.1093/brain/awaa080 (2020). [PubMed: 32419025]
14. Elitt MS et al. Chemical Screening Identifies Enhancers of Mutant Oligodendrocyte Survival and Unmasks a Distinct Pathological Phase in Pelizaeus-Merzbacher Disease. Stem Cell Reports 11, 711–726, doi:10.1016/j.stemcr.2018.07.015 (2018). [PubMed: 30146490]
15. Southwood CM, Garbern J, Jiang W & Gow A The unfolded protein response modulates disease severity in Pelizaeus-Merzbacher disease. Neuron 36, 585–596 (2002). [PubMed: 12441049]
16. Jinek M et al. A programmable dual-RNA-guided DNA endonuclease in adaptive bacterial immunity. Science 337, 816–821, doi:10.1126/science.1225829 (2012). [PubMed: 22745249]
17. Cong L et al. Multiplex genome engineering using CRISPR/Cas systems. Science 339, 819–823, doi:10.1126/science.1231143 (2013). [PubMed: 23287718]
18. Tatar CL et al. Increased Plp1 gene expression leads to massive microglial cell activation and inflammation throughout the brain. ASN Neuro 2, e00043, doi:10.1042/AN20100016 (2010). [PubMed: 20885931]
19. Uschkureit T, Sporkel O, Bussow H & Stoffel W Rumpshaker-like proteolipid protein (PLP) ratio in a mouse model with unperturbed structural and functional integrity of the myelin sheath and axons in the central nervous system. Glia 35, 63–71, doi:10.1002/glia.1071 (2001). [PubMed: 11424193]
20. Finkel RS et al. Nusinersen versus Sham Control in Infantile-Onset Spinal Muscular Atrophy. N Engl J Med 377, 1723–1732, doi:10.1056/NEJMoa1702752 (2017). [PubMed: 29091570]
21. Kordasiewicz HB et al. Sustained therapeutic reversal of Huntington's disease by transient repression of huntingtin synthesis. Neuron 74, 1031–1044, doi:10.1016/j.neuron.2012.05.009 (2012). [PubMed: 22726834]
22. Mazur C et al. Brain pharmacology of intrathecal antisense oligonucleotides revealed through multimodal imaging. JCI Insight 4, doi:10.1172/jci.insight.129240 (2019).
23. Wu Q et al. Elevated levels of the chemokine GRO-1 correlate with elevated oligodendrocyte progenitor proliferation in the jimpy mutant. J Neurosci 20, 2609–2617 (2000). [PubMed: 10729341]
24. Miller MJ et al. Proteolipid protein gene mutation induces altered ventilatory response to hypoxia in the myelin-deficient rat. The Journal of neuroscience : the official journal of the Society for Neuroscience 23, 2265–2273 (2003). [PubMed: 12657685]
25. Ueda A et al. Pelizaeus-Merzbacher disease can be a differential diagnosis in males presenting with severe neonatal respiratory distress and hypotonia. Hum Genome Var 5, 18013, doi:10.1038/hgv.2018.13 (2018). [PubMed: 29619238]
26. Osorio MJ et al. Concise Review: Stem Cell-Based Treatment of Pelizaeus-Merzbacher Disease. Stem Cells 35, 311–315, doi:10.1002/stem.2530 (2017). [PubMed: 27882623]
27. Renier WO et al. Connatal Pelizaeus-Merzbacher disease with congenital stridor in two maternal cousins. Acta Neuropathol 54, 11–17, doi:10.1007/bf00691328 (1981). [PubMed: 7234326]
28. Lee Y et al. Oligodendroglia metabolically support axons and contribute to neurodegeneration. Nature 487, 443–448, doi:10.1038/nature11314 (2012). [PubMed: 22801498]
29. Funfschilling U et al. Glycolytic oligodendrocytes maintain myelin and long-term axonal integrity. Nature 485, 517–521, doi:10.1038/nature11007 (2012). [PubMed: 22622581]
30. Freeman SA et al. Acceleration of conduction velocity linked to clustering of nodal components precedes myelination. Proceedings of the National Academy of Sciences of the United States of America 112, E321–328, doi:10.1073/pnas.1419099112 (2015). [PubMed: 25561543]
31. Nave KA, Lai C, Bloom FE & Milner RJ Jimpy mutant mouse: a 74-base deletion in the mRNA for myelin proteolipid protein and evidence for a primary defect in RNA splicing. Proc Natl Acad Sci U S A 83, 9264–9268, doi:10.1073/pnas.83.23.9264 (1986). [PubMed: 3466187]
32. Hsu PD et al. DNA targeting specificity of RNA-guided Cas9 nucleases. Nat Biotechnol 31, 827–832, doi:10.1038/nbt.2647 (2013). [PubMed: 23873081]

33. Nakagata N, Okamoto M, Ueda O & Suzuki H Positive effect of partial zona-pellucida dissection on the in vitro fertilizing capacity of cryopreserved C57BL/6J transgenic mouse spermatozoa of low motility. Biol Reprod 57, 1050–1055 (1997). [PubMed: 9369169]
34. Schmid-Burgk JL et al. OutKnocker: a web tool for rapid and simple genotyping of designer nuclease edited cell lines. Genome Res 24, 1719–1723, doi:10.1101/gr.176701.114 (2014). [PubMed: 25186908]
35. Li H & Durbin R Fast and accurate short read alignment with Burrows-Wheeler transform. Bioinformatics 25, 1754–1760, doi:10.1093/bioinformatics/btp324 (2009). [PubMed: 19451168]
36. Stemmer M, Thumberger T, Del Sol Keyer M, Wittbrodt J & Mateo JL CCTop: An Intuitive, Flexible and Reliable CRISPR/Cas9 Target Prediction Tool. PLoS One 10, e0124633, doi:10.1371/journal.pone.0124633 (2015). [PubMed: 25909470]
37. Bae S, Park J & Kim JS Cas-OFFinder: a fast and versatile algorithm that searches for potential off-target sites of Cas9 RNA-guided endonucleases. Bioinformatics 30, 1473–1475, doi:10.1093/bioinformatics/btu048 (2014). [PubMed: 24463181]
38. Haeussler M et al. Evaluation of off-target and on-target scoring algorithms and integration into the guide RNA selection tool CRISPOR. Genome Biol 17, 148, doi:10.1186/s13059-016-1012-2 (2016). [PubMed: 27380939]
39. Robinson JT et al. Integrative genomics viewer. Nature biotechnology 29, 24–26, doi:10.1038/nbt.1754 (2011).
40. Wisniewski JR, Zougman A, Nagaraj N & Mann M Universal sample preparation method for proteome analysis. Nat Methods 6, 359–362, doi:10.1038/nmeth.1322 (2009). [PubMed: 19377485]
41. Tran NH et al. Deep learning enables de novo peptide sequencing from data-independent-acquisition mass spectrometry. Nat Methods 16, 63–66, doi:10.1038/s41592-018-0260-3 (2019). [PubMed: 30573815]
42. Tran NH, Zhang X, Xin L, Shan B & Li M De novo peptide sequencing by deep learning. Proc Natl Acad Sci U S A 114, 8247–8252, doi:10.1073/pnas.1705691114 (2017). [PubMed: 28720701]
43. Najm FJ et al. Rapid and robust generation of functional oligodendrocyte progenitor cells from epiblast stem cells. Nature methods 8, 957–962, doi:10.1038/nmeth.1712 (2011). [PubMed: 21946668]
44. Lager AM et al. Rapid functional genetics of the oligodendrocyte lineage using pluripotent stem cells. Nat Commun 9, 3708, doi:10.1038/s41467-018-06102-7 (2018). [PubMed: 30213958]
45. Hagemann TL et al. Antisense suppression of glial fibrillary acidic protein as a treatment for Alexander disease. Ann Neurol 83, 27–39, doi:10.1002/ana.25118 (2018). [PubMed: 29226998]
46. Glascock JJ et al. Delivery of therapeutic agents through intracerebroventricular (ICV) and intravenous (IV) injection in mice. J Vis Exp, doi:10.3791/2968 (2011).

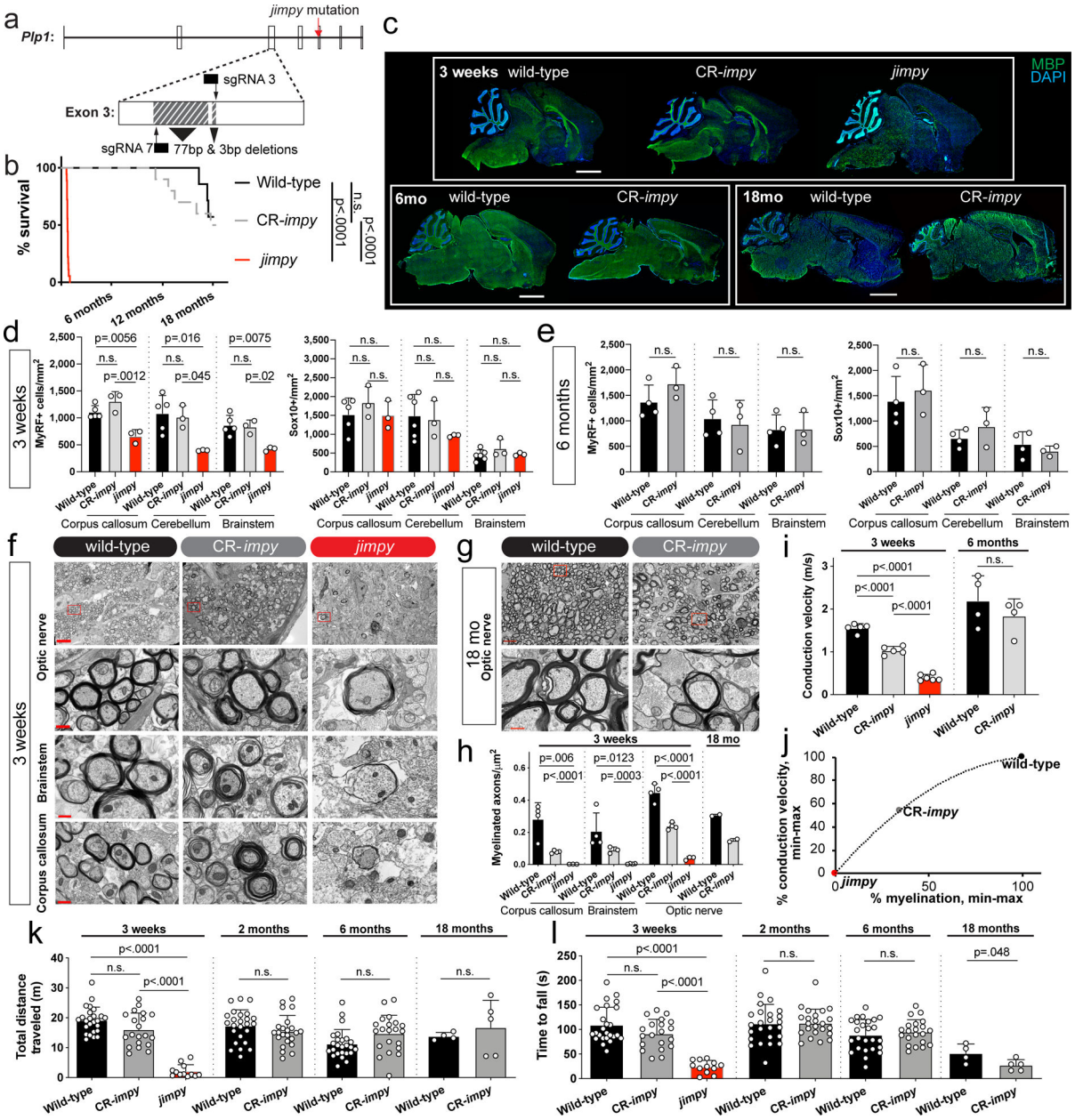

Fig. 1 |. Germline *Plp1* suppression in *jimpy* rescues lifespan and restores functional myelin.

a, Schematic of CRISPR *Plp1* targeting in *jimpy*. Black arrows indicate predicted sgRNA cutting sites. Hashed boxes show the CR-*impy* 80 base-pair complex deletion (see Extended Data Fig. 1a). **b**, Kaplan-Meier plot comparing lifespans between genotypes. n=25, 23, 18 for wild-type, CR-*impy*, and *jimpy* mice, respectively. p-values calculated using log-rank test. For source data, see Supplementary Data 1. **c**, Immunohistochemical images of whole-brain sagittal sections showing MBP$^+$ myelin (green) and DAPI$^+$ nuclei (blue). Scale bars, 2mm. **d-e**, Quantification of MyRF$^+$ and Sox10$^+$ cells at (**d**) 3 weeks and (**e**) 6 months. n=3–6 mice. For representative source images, see Supplementary Data 3–5. **f-g**, Electron micrograph images showing myelination at (**f**) 3 weeks and (**g**) 18 months. Higher magnification of red boxed area shown in subsequent row. Scale bar, 0.5μm; except first row,

5μm. **h**, Quantification of myelinated axons at 3 weeks (n=3–4 mice) and 18 months (n=2 mice). p-values calculated with unpaired, two-sided t-tests. **i**, Optic nerve conduction velocities at 3 weeks (n=5–6 mice) and 6 months (n=4 mice). **j**, Polynomial trendline illustrating conduction velocity *vs*. brain myelination in CR-*impy* relative to min-max scaling of values from *jimpy* and wild-type. Data from 3-week time point of (**h**) and (**i**), with same n. **k-l**, (**k**) Accelerating rotarod or (**l**) open field performance. n=25, 20, 12 (3 weeks) for wild-type, CR-*impy*, *jimpy* mice, respectively. n= 25, 23 (2 months); n=25, 21 (6 months); n=4, 5 (18 months) mice for wild-type, CR-*impy*, respectively.
Biological replicates (individual mice) indicated by open circles. Graph bars indicate mean ± standard deviation. p-values calculated using one-way ANOVA with Tukey correction at 3 weeks or two-way, an unpaired two-sided t-test at later time points, except where indicated. p-values stated for $p<0.1$, otherwise not significant (n.s).

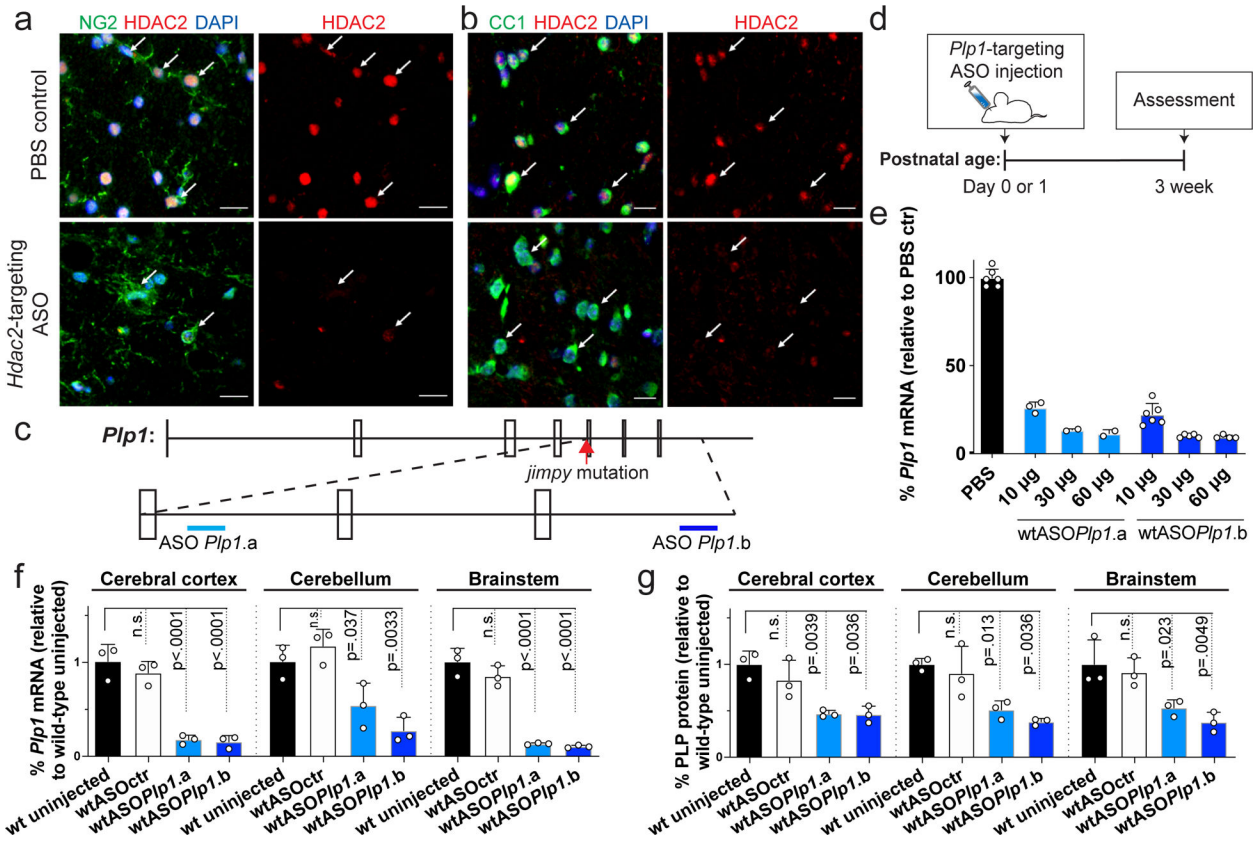

Fig. 2 |. Efficient ASO-mediated transcript suppression in OPCs and oligodendrocytes *in vivo*.

a-b, Immunostaining of HDAC2$^+$ (red) and (**a**) NG2$^+$ OPCs (green; arrows) in the spinal cord or (**b**) CC1$^+$ oligodendrocytes (green; arrows) in the corpus callosum from 8-week-old wild-type mice injected with PBS control or *Hdac2*-targeting ASO, 2 weeks post-injection. Scale bar, 20 µm. **c**, Depiction of *Plp1* pre-mRNA demonstrating the approximate binding locations of two independent ASOs in intron 5 and the 3' UTR. **d**, Schematic of the design for ASO experiments in this figure. **e**, RT-qPCR data showing wild-type spinal cord *Plp1* transcript levels, 3 weeks after injection with the indicated ASO doses (10µg, 30µg, and 60µg) or PBS controls at postnatal day 1 (n=2–6 mice). **f**, RT-qPCR data showing the levels of *Plp1* transcript and **g**, western blot data showing the levels of PLP protein, 3 weeks post-ASO injection (30µg dose) at birth in wild-type (n=3 mice).

Individual data points represent the mean value of 4 technical replicates for each biological replicate (**e, f**) or independent biological replicates (**g**). Biological replicates (individual mice) indicated by open circles. Graph bars indicate mean ± standard deviation. p-values calculated using one-way ANOVA with Dunnett's correction. p-values stated for p<0.1, otherwise not significant (n.s). See Supplementary Data 4 for full western blot source images.

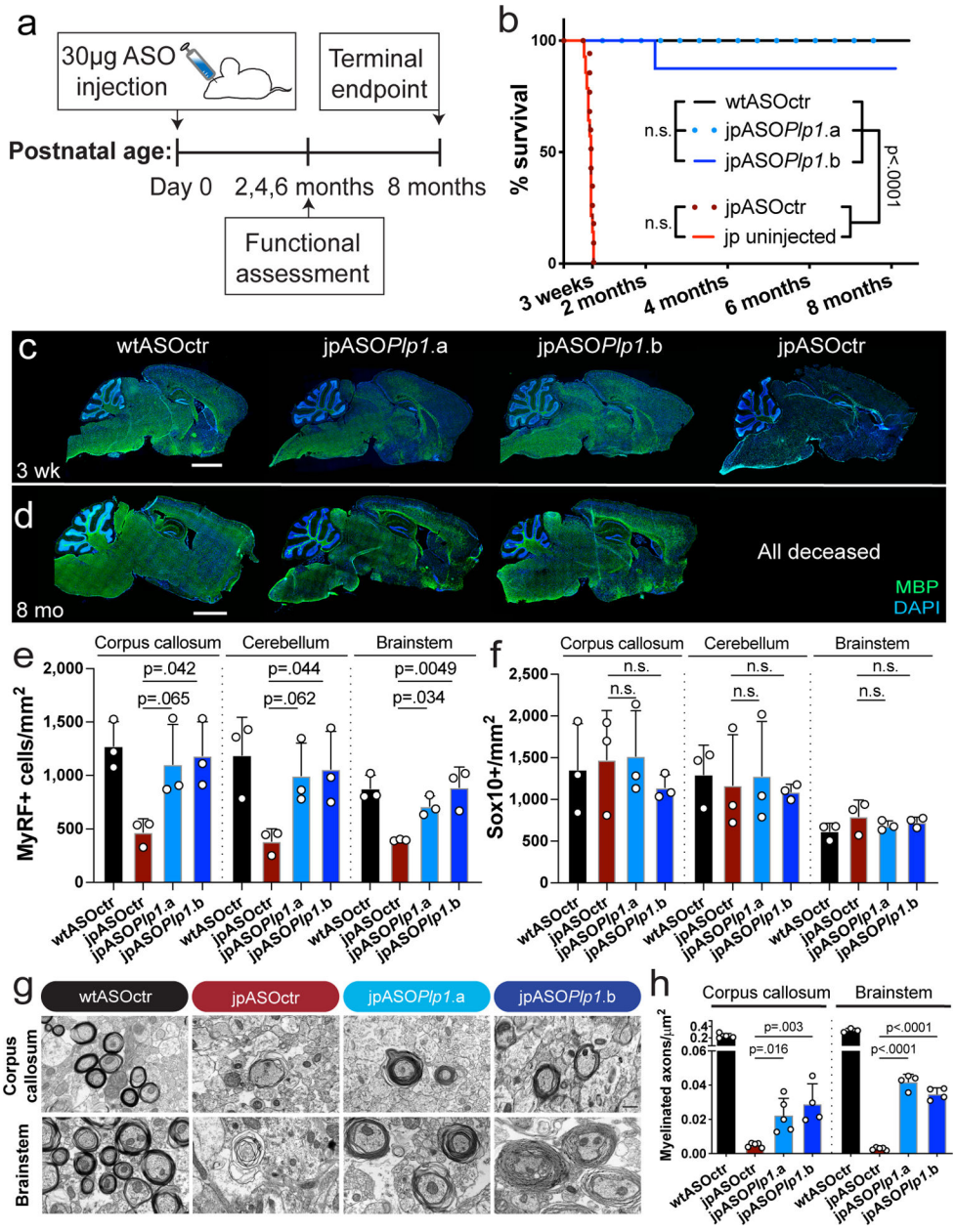

Fig. 3 |. Postnatal delivery of *Plp1*-targeted antisense oligonucleotides rescues lifespan and oligodendrocytes with partial restoration of myelin in *jimpy*.

a, Schematic of ASO experimental design used in Figures 3-4. **b**, Kaplan-Meier plot depicting the lifespan of contemporaneous wtASOctr, uninjected *jimpy*, jpASOctr, jpASO*Plp1*.a, and jpASO*Plp1*.b (n=12, 14, 5, 5 mice, respectively). p-values calculated using the log-rank test. See Supplementary Data 6 for source metadata. **c-d**, Immunohistochemical images of (**c**) 3-week and (**d**) 8-month whole-brain sagittal sections showing MBP$^+$ myelin (green) and DAPI$^+$ nuclei (blue) staining. Scale bar, 2mm. See Supplementary Data 8–10 for higher magnification. **e-f**, Quantification of (**e**) MyRF$^+$ oligodendrocytes and (**f**) Sox10$^+$ glial lineage cells at 3 weeks of age (n=3 mice). For representative source images, see Supplementary Data 8–10. **g-h**, (**g**) Electron micrograph

images and (**h**) quantification of myelinated axons at 3 weeks of age (n=3–5 mice). Scale bar, 0.5μm.

Biological replicates (individual mice) indicated by open circles. Graph bars indicate mean ± standard deviation. p-values calculated using one-way ANOVA with Dunnett's correction, except where indicated. p-values stated for $p<0.1$, otherwise not significant (n.s).

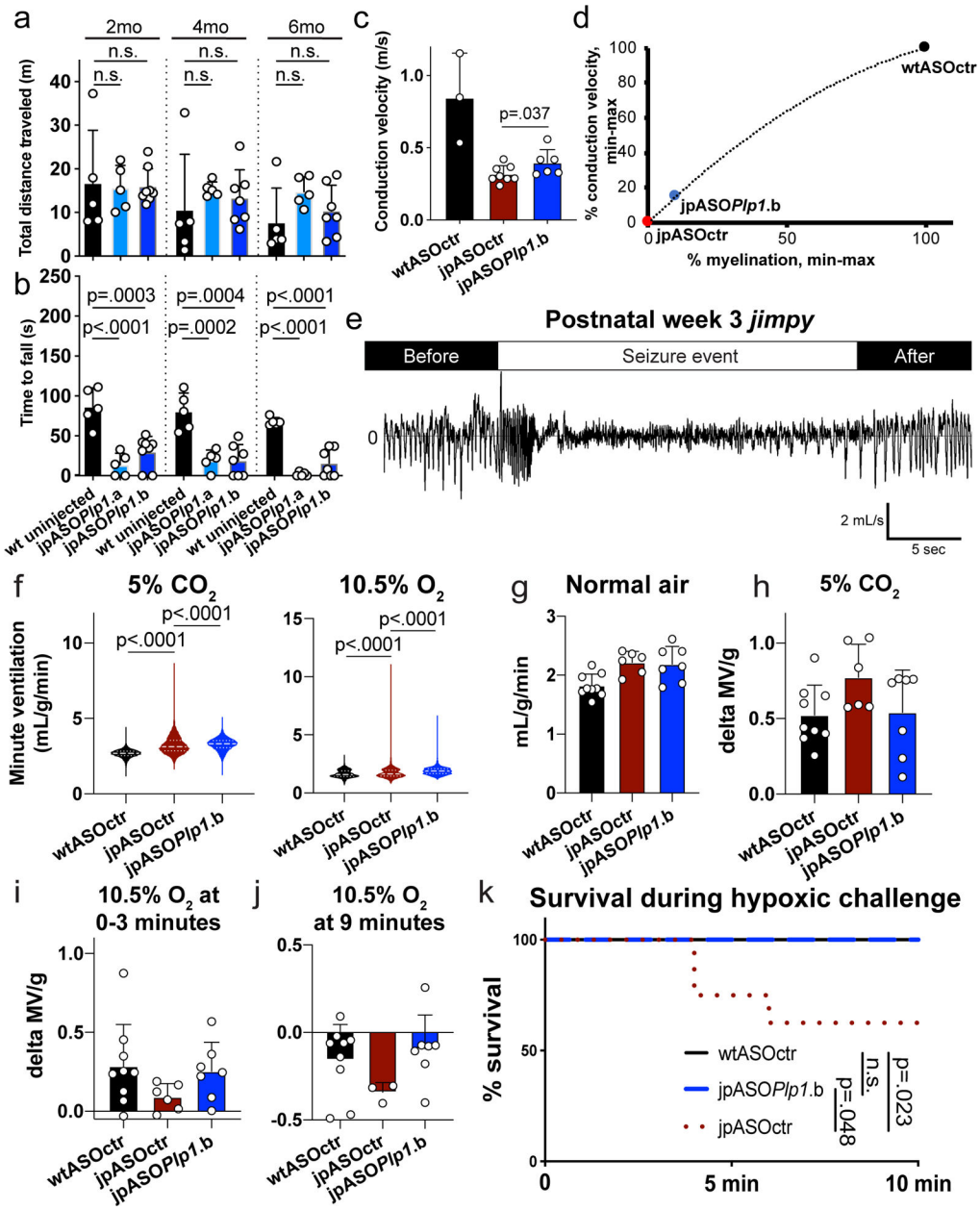

Fig. 4 |. ASO-mediated *Plp1* suppression in *jimpy* leads to functional myelin, improved control of respiratory function, and prevention of hypoxia-induced mortality.

a-b, Performance for (**a**) open field testing (**b**) accelerating rotarod (n=5–8 mice). See Supplementary Data 6 for raw data values. p-values calculated using one-way ANOVA with Dunnett's correction. **c**, Optic nerve conduction velocity at 3 weeks of age (n = 3, 8, and 4 wtASOctr, jpASOctr, and jpASO*Plp1*.b mice, respectively). p-values calculated using one-sided, unpaired t-test. **d**, Polynomial trendline illustrating conduction velocity *vs.* brain myelination in jpASO*Plp1*.b relative to min-max scaling of values from jpASOctr and wtASOctr. Source data from (**c** and Fig. 3h) with same n. **e**, Trace of a *jimpy* seizure during hypercapnic challenge (respiratory flow rate on y-axis). **f**, Minute ventilation per body weight (MV/g) in mL/g/min in 5% CO_2 (hypercapnia) and 10.5% O_2 (hypoxia),

representing all repeated measurements from n=9, 6, 7 wtASOctr, jpASOctr, and jpASO*Plp1*.b mice, respectively. Violin plots indicate median (center white lines) ± quartiles (border white lines). p-values calculated using Brown and Forsythe's test. **g-j**, Baseline MV/g (mL/g/min) in (**g**) normal air, (**h**) 15–30 minutes after transitioning from normal air to 5% CO_2, (**i**) 0–3 minutes and (**j**) 8–9 minutes after transitioning from normal air to 10.5% O_2. Post-mortality hypoxia data were not included. For g-i, n=9, 6, 7 and j, n=9, 3, 7 wtASOctr, jpASOctr, and jpASO*Plp1*.b mice, respectively. **k**, Kaplan-Meier plot depicting survival during hypoxia. n=12, 8, 9 wtASOctr, jpASOctr, and jpASO*Plp1*.b mice, respectively. p-values calculated using log-rank test.

Biological replicates (individual mice) indicated by open circles. Graph bars indicate mean ± standard deviation, except where indicated. p-values stated for $p<0.1$, otherwise not significant (n.s).